

Development of Metal Sulfide Base Nanostructured Anode Material for Li-Ion Batteries



By

Muhammad Arslan

(Registration No: 00000400321)

Department of Materials Engineering

School of Chemical and Materials Engineering

National University of Sciences & Technology (NUST)

Islamabad, Pakistan

(2024)

Development of Metal Sulfide Base Nanostructured Anode Material for Li-Ion Batteries



By

Muhammad Arslan

(Registration No: 00000400321)

A thesis submitted to the National University of Sciences and Technology, Islamabad,

in partial fulfillment of the requirements for the degree of

Master of Science in
Nanoscience and Engineering

Supervisor: Dr. Amna Safdar

Co Supervisor: Dr. Mashkoor Ahmad

School of Chemical and Materials Engineering

National University of Sciences & Technology (NUST)

Islamabad, Pakistan

(2024)

THESIS ACCEPTANCE CERTIFICATE



THESIS ACCEPTANCE CERTIFICATE

Certified that final copy of MS Thesis entitled "Development of Metal Sulfide Base Nanostructured Anode Materials for Li-Ion Batteries" written by Mr Muhammad Arslan (Registration No 00000400321), of School of Chemical & Materials Engineering (SCME) has been vetted by undersigned, found complete in all respects as per NUST Statues/Regulations, is free of plagiarism, errors, and mistakes and is accepted as partial fulfillment for award of MS degree. It is further certified that necessary amendments as pointed out by GEC members of the scholar have also been incorporated in the said thesis.

Signature: _____

Name of Supervisor: Dr Amna Safdar

Date: 08-10-2024

Signature (HOD): _____

Date: _____

Signature (Dean/Principal): _____

Date: _____

TH - 1

NSE-10-2022


Form TH-1

National University of Sciences & Technology (NUST)
MASTER'S THESIS WORK
Formulation of Guidance and Examination Committee (GEC)


Name: Muhammad Arslan NUST Reg No: 00000400321
Department: Department of Materials Engineering Specialization: Master of Science in Nanoscience and Engineering
Credit Hour Completed: 24.0 CGPA: 3.88

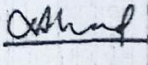
Course Work Completed

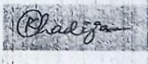
S/No:	Code:	Title:	Core/Elective:	CH:	Grade:
1.	MSE-854	Characterization Of Materials	Compulsory	3.0	A
2.	NSE-813	Essentials of Nanoscience and Engineering	Compulsory	3.0	A
3.	RM-898	Research Methodology	Additional	2.0	Q
4.	NSE-843	Nano Technology And Photovoltaics	Elective	3.0	A
5.	MSE-856	Nano Material and Processing	Compulsory	3.0	A
6.	NSE-812	Environmental Nanotechnology	Elective	3.0	A
7.	NSE-941	Nano Composite Materials	Elective	3.0	B+
8.	ESE-836	Li-ion and Next Generation Batteries	Elective	3.0	B+
9.	NSE-845	Nanolithography And Device Fabrication	Elective	3.0	A

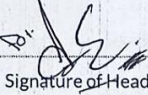
Date 02 - Jan - 2024 Student's Signature: 

Thesis Committee

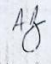
1. Name: Amna Safdar (Supervisor) Signature: 
Department: Department of Materials Engineering

2. Name: Nasir Mahmood Ahmad (Internal) Signature: 
Department: Department of Materials Engineering

3. Name: Khadija Munawar (Internal) Signature: 
Department: Department of Chemistry

4. Dr. Mashkook Ahmed (Co-Supervisor) Signature of Head of Department: 
Date: 02-Jan-2024

APPROVAL

Date: 02 - Jan - 2024 Signature of Dean/Principal: 

School of Chemical & Materials Engineering (SCME) H-12 Campus

TH - 4



National University of Sciences & Technology (NUST)

FORM TH-4

MASTER'S THESIS WORK

We hereby recommend that the dissertation prepared under our supervision by

Regn No & Name: 00000400321 Muhammad Arslan

Title: Development of Metal Sulfide Base Nanostructured Anode Material for Li-Ion Batteries.

Presented on: 03 Oct 2024 at: 1530 hrs in SCME Seminar Hall

Be accepted in partial fulfillment of the requirements for the award of Master of Science degree in Nanoscience & Engineering.

Guidance & Examination Committee Members

Name: Dr Nasir M. Ahmed

Signature: *N. Ahmed*

Name: Dr Khadija Munawar

Signature: *Khadija 3/10/24*

Name: Dr Mashkoor Ahmad (Co-Supervisor)

Signature: *M. Ahmad*

Supervisor's Name: Dr Amna Safdar

Signature: *A. Safdar*

Dated: 07/10/2024

[Signature]
Head of Department

Date 7/10/24

[Signature]
Dean/Principal

Date 10/13/24
od.

AUTHOR'S DECLARATION

I **Muhammad Arslan** hereby state that my MS thesis titled “**Development of Metal Sulfide Base Nanostructured Anode Material for Li-Ion Batteries**” is my own work and has not been submitted previously by me for taking any degree from National University of Sciences and Technology, Islamabad or anywhere else in the country/ world.

At any time if my statement is found to be incorrect even after I graduate, the university has the right to withdraw my MS degree.

Name of Student: Muhammad Arslan

Date: 08 October 2024

PLAGIARISM UNDERTAKING

I solemnly declare that research work presented in the thesis titled “Development of Metal Sulfide Base Nanostructured Anode Material for Li-Ion Batteries” is solely my research work with no significant contribution from any other person. Small contribution/ help wherever taken has been duly acknowledged and that complete thesis has been written by me.

I understand the zero-tolerance policy of the HEC and National University of Sciences and Technology (NUST), Islamabad towards plagiarism. Therefore, I as an author of the above titled thesis declare that no portion of my thesis has been plagiarized and any material used as reference is properly referred/cited.

I undertake that if I am found guilty of any formal plagiarism in the above titled thesis even after award of MS degree, the University reserves the rights to withdraw/revoke my MS degree and that HEC and NUST, Islamabad has the right to publish my name on the HEC/University website on which names of students are placed who submitted plagiarized thesis.

Student Signature: 

Name: Muhammad Arslan

DEDICATION

*"I dedicated this thesis work to Allah **"The Creator"** (SubhanahuWaTa'ala) almighty, my beloved mother, siblings and cherished moments with my late father **"Elahi Bakhsh"** and Sir **"Ibrahim Khalil"** whose love, presence and unwavering support have been the cornerstones of my life. I am certain they would be filled with immense joy to witness my achievement of completing a Master in Nanoscience Engineering from SCME (NUST). I cherish every memory and lesson they bestowed upon me, and I carry their spirit in every challenge I overcome.*

*I extend profound gratitude to my Sir **"Dr. Hammad Moeen Arbi"** whose support and wise counsel have been pillars of strength during my academic endeavor. My journey would not have been the same without the companionship and support of my elder brother **"Muhammad Farhan"** and my elder sister **"Saima Malik"** and **"Aqsa Manzoor"** You all have been my support system, providing love and motivation that have been crucial to my success.*

*Finally, I expressed my special gratitude to my esteemed supervisor, **"Dr. Amna Safdar"** whose expertise and meticulous guidance have been instrumental in sculpting this research work. Her patience and dedication to excellence have not only shaped this thesis but have also greatly influenced my personal and professional growth. Lastly, I would like to express my sincere thanks to **"Ms. Momna Haq"** (Master fellow SCME) and **Mr. Zahid Abbas** (Research fellow PINSTECH), I am grateful for your collaborative spirit and efforts throughout my research work. I am immensely thankful to all my peers and friends at SCME as well as PINSTECH. To all of you, thank you for being a part of this journey."*

ACKNOWLEDGEMENTS

I am very humbled and blessed that *Allah “The Creator” (SubhanahuWaTa’ala)* has been very kind and merciful, for giving me strength, guidance and patience to complete this research work. I am grateful to Allah Almighty for blessing me with knowledge, health and strength, which empowered me to accomplish my thesis. I am thankful to my wife for her support and love in taking all the burden of family affairs and giving me space for the timely completion of this research work. My siblings whose prayers and moral support have encouraged me during the journey.

I am grateful to my supervisor “*Dr. Amna Safdar*” for her great support, help and supervision throughout this period. Her valuable guidance has been a cornerstone of my research and has allowed me to overcome numerous challenges. I am equally thankful to my mentor and co-supervisor, “*Dr. Mashkoor Ahmad*” and “*Dr. Amjad Nisar*” from PINSTECH, for offering me the opportunity to work in a prestigious national research institute, where his insights and advice greatly shaped my work. His encouragement, alongside full access to lab facilities, made a significant impact on the progress of this research.

I would also like to express my sincere appreciation to the members of my Guidance and Examination Committee (GEC), “*Prof. Dr. Nasir Mahmood Ahmad*” and “*Dr. Khadija Munawar*” for their valuable comments and suggestions as it help me to polish my thesis. I would like to extend my heartfelt gratitude to all the lab engineers, faculty and staff at the School of Chemical and Materials Engineering (SCME) for their invaluable support and encouragement, which have greatly contributed to the successful completion of this research, Also sincere thanks to “Mr. Altaf Hussain, Mr. Abdur Rehman Khan Niazi, Mr. Peer Muhammad, Mr. Ammar Ud din NSE-10, Mr. Marghoob Ahmad NSE-09, Mr. Rehan Ullah MSE-16, Mr. Samee-Ullah IESE, , Mr. Shoaib Bilal GCUL and Mr. Shakeel Abbas from GCUF” for their dedicated and selfless support during my research work.

Muhammad Arslan

TABLE OF CONTENTS

ACKNOWLEDGEMENTS	IX
TABLE OF CONTENTS	X
LIST OF TABLES	XIII
LIST OF FIGURES	XIV
LIST OF SYMBOLS, ABBREVIATIONS AND ACRONYMS	XVI
ABSTRACT	XVIII
CHAPTER 1: INTRODUCTION	1
1.1 Motivation	1
1.2 Background	2
1.2.1 <i>Energy Storage Systems (ESS) Overview</i>	3
1.2.2 <i>Indirect Storage</i>	3
• 1.2.3 <i>Direct Storage</i>	3
1.2.4 <i>Battery vs Supercapacitors</i>	4
1.3 Battery	5
1.3.1 <i>Primary Batteries Vs Secondary Batteries</i>	6
1.3.2 <i>Lithium-Ion batteries (LIBs)</i>	7
1.3.3 <i>History of Li-Ion batteries (LIBs)</i>	9
1.3.4 <i>Why Rocking Chair batteries?</i>	10
1.3.5 <i>Applications of Li-ion batteries</i>	12
1.3.6 <i>Working Principle of Li-ion batteries</i>	14
1.3.7 <i>Material attributes</i>	15
1.3.8 <i>Anode</i>	16
1.3.9 <i>Cathode</i>	16
1.3.10 <i>Electrolyte</i>	16
1.3.11 <i>Separator</i>	17
1.4 Limitations of Li-ion batteries	18
1.4.1 <i>Low Power Density</i>	18
1.4.2 <i>Safety Concerns / Explosive</i>	18
1.4.3 <i>Cost</i>	18
1.4.4 <i>Temperature Window</i>	19
1.4.5 <i>Supply and demand</i>	19
1.4.6 <i>Aging and Performance Degradation</i>	19
1.5 What is SnS?	20
1.5.1 <i>Structure of SnS</i>	21
1.5.2 <i>Advantages of SnS</i>	22
1.5.3 <i>Disadvantages of SnS</i>	22
1.6 What is ZnS?	23

1.6.1	<i>Structure of ZnS</i>	24
1.6.2	<i>Lattice Orientation</i>	24
1.6.3	<i>Advantages of ZnS</i>	25
1.6.4	<i>2 Disadvantages of ZnS</i>	25
1.7	Significance and Research Objectives	25
1.8	Research Objectives	26
CHAPTER 2: LITERATURE REVIEW		27
2.1	Historical Background	27
2.2	Common Anode Materials for Lithium-Ion Batteries	28
2.2.1	<i>Requirements of Anode Material</i>	28
2.2.2	<i>Commercialized anode: Graphite, Hard Carbons</i>	29
2.2.3	<i>Intercalation Types</i>	29
2.2.4	<i>Conversion Types</i>	30
2.2.5	<i>Alloy Types</i>	31
2.3	Why SnS and ZnS as an Electrode Material	32
2.3.1	<i>High Theoretical Capacity and Energy Density</i>	32
2.3.2	<i>Volume Expansion</i>	32
2.3.3	<i>Cost and Abundance</i>	32
2.3.4	<i>Cycle Life</i>	32
2.3.5	<i>Tuneability and Safety</i>	33
2.4	Composite and Nanostructured in SnS Anode Material	33
2.5	Composite and Nanostructured in ZnS Anode Material	36
2.6	Binary Metal Sulfide Based Composites	38
CHAPTER 3: MATERIALS AND METHODS		42
3.1	Reagents and Chemicals	42
3.2	Synthesis of Material	42
3.2.1	<i>Synthesis of ZnS</i>	42
3.2.2	<i>Synthesis of SnS</i>	43
3.2.3	<i>Synthesis of SnS:ZnS Composite</i>	44
3.2.4	<i>Synthesis of Graphitic Carbon Nitride</i>	46
3.2.5	<i>Synthesis of SnS:ZnS@ g-C₃N₄</i>	46
3.3	Fabrication of Electrodes	47
3.3.1	<i>Slurry Preparation</i>	47
3.3.2	<i>Electrode Coating</i>	48
3.3.3	<i>Electrode Calendaring</i>	49
3.3.4	<i>Electrode Punching</i>	49
3.4	Assembling of Cells	50
CHAPTER 4: CHARACTERIZATION		54
4.1	Structural, Morphological and Compositional Analysis	54
4.1.1	<i>X-Ray Diffraction Analysis (XRD)</i>	54
4.1.2	<i>SEM Analysis</i>	55
4.1.3	<i>FTIR Analysis</i>	57
4.1.4	<i>XPS Analysis</i>	58
4.2	Electrochemical Measurements	60

4.2.1	<i>Cyclic Voltammetry</i>	60
4.2.2	<i>Galvanostatic Charging and Discharging (GCD)</i>	61
4.2.3	<i>Rate Performance</i>	62
4.2.5	<i>Cyclic stability</i>	63
4.2.5	<i>EIS Testing</i>	65
4.3	Density Functional Theory (DFT)	66
4.3.1	<i>Siesta Calculations</i>	67
4.3.2	<i>Electrical Properties of ZnS by Siesta</i>	67
4.3.3	<i>Electrical Properties of SnS by Siesta</i>	68
4.3.4	<i>Heterostructure of SnS:ZnS</i>	69
CHAPTER 5: CONCLUSIONS AND FUTURE RECOMMENDATION		71
5.1	Conclusion	71
5.2	Future Recommendations	71
REFERENCES		72

LIST OF TABLES

Table 1.1: Comparison Between Primary and Secondary Batteries.	6
Table 1.2: Performance comparison of different batteries.	12
Table 1.3: Chemical and Electrical Properties of SnS	21
Table 1.4: Chemical and Electrical Properties of ZnS	23
Table 2.1: Literature survey of SnS:ZnS based composites.	39
Table 4.1: EIS fitting parameters of ZnS, SnS, SnS:ZnS and SnS:ZnS@g-C ₃ N ₄ electrodes.....	66

LIST OF FIGURES

Figure 1.1: Ragon-plot showing the performance domain of various types electrochemical energy- storage devices compared to internal-combustion gas engine [3].	2
Figure 1.2: Simple Battery Setup.....	5
Figure 1.3: Standard Reduction Potential of different elements at 25 °C [16]	8
Figure 1.4: Nobel laureate in Chemistry (Li-Ion batteries) [23].....	10
Figure 1.5: Charge and Discharge Phenomena of Lithium ion Batteries [29]	15
Figure 1.6: Flow Chart Diagram of Limitations of Li-Ion Batteries.	20
Figure 1.7: Orthorhombic Structure of SnS.....	22
Figure 1.8: Cubic Structure of SnS.....	24
Figure 2.1: Graphite battery mechanism.....	27
Figure 2.2: Specific Capacity and Operating Voltage of Various Anode [47].....	28
Figure 2.3: Mechanism of Intercalation Type Anode Material [49].....	29
Figure 2.4: Mechanism of Conversion Type Anode Material [49].	30
Figure 2.5: Mechanism of Alloy Type Anode Material [49].....	31
Figure 3.1: Schematic Illustration of ZnS Synthesis.	43
Figure 3.2: Schematic Illustration of SnS Synthesis.....	44
Figure 3.3: Schematic Illustration of Synthesis of SnS-ZnS	45
Figure 3.4: Schematic Illustration Synthesis of g-C ₃ N ₄	46
Figure 3.5: Schematic Illustration of SnS:ZnS@g-C ₃ N ₄	47
Figure 3.6: Slurry Preparation	48
Figure 3.7: Representations of Pasted Slurry on a Cu Foil.....	48
Figure 3.8: Representations of Calendaring Process	49
Figure 3.9: Representations of Electrode Cutting After Proper Drying	49
Figure 3.10: Flow Diagram of Electrodes Fabrication Process	50
Figure 3.11: Coin cell fabrication process in a glove box.	51
Figure 3.12: Steps for coin cell assembly.	52
Figure 4.1: XRD spectra of g-C ₃ N ₄ sheets	55
Figure 4.2: XRD Spectra of ZnS, SnS, SnS:ZnS and SnS:ZnS@g-C ₃ N ₄	55
Figure 4.3: Lower and higher magnification SEM images of g-C ₃ N ₄ 2D sheets (a, b) SnS:ZnS nanoparticles (c) Incorporation of SnS:ZnS on g-C ₃ N ₄ 2D sheets (d).....	56
Figure 4.4: EDX spectra of g-C ₃ N ₄ 2D sheets (a) and SnS:ZnS on g-C ₃ N ₄	57
Figure 4.5: FTIR spectra of g-C ₃ N ₄ , SnS, ZnS, SnS:ZnS and SnS:ZnS@g-C ₃ N ₄ composite	58
Figure 4.6: Higher Resolution XPS spectra (a) Sn 3d (b) Zn 2p (c) C 1s (d) S 2p (e) N 1s	59
Figure 4.7: CV curves of SnS:ZnS on g-C ₃ N ₄ at scan rate of 0.5 mVs ⁻¹	61
Figure 4.8: Galvanostatic charge-discharge curve of SnS:ZnS@g-C ₃ N ₄	62
Figure 4.9: Rate capability comparison of ZnS, SnS, SnS:ZnS and SnS:ZnS@g-C ₃ N ₄ electrodes at various C-rates where 0.3C= 614 mAhg ⁻¹	63

Figure 4.10: Cyclic performance comparison of ZnS, SnS, SnS:ZnS and SnS:ZnS@g-C ₃ N ₄ electrodes at 0.3C	64
Figure 4.11: Prolong cyclic performance of SnS:ZnS@g-C ₃ N ₄ at 0.3C for 1000 cycles.	65
Figure 4.12: EIS Nyquist plot of pure SnS (red), ZnS (green), SnS:ZnS (blue) and SnS:ZnS@g-C ₃ N ₄ (black) electrode calculated over the AC frequency range from 0.01 Hz to 100 kHz (a) and RC fitted equivalent circuit (b).....	65
Figure 4.13: PDOS of pure ZnS (a) Bandgap of ZnS (b)	67
Figure 4.14: PDOS of pure SnS (a) Bandgap of SnS (b).....	69
Figure 4.15: Heterostructure of SnS:ZnS	70

LIST OF SYMBOLS, ABBREVIATIONS AND ACRONYMS

LIBs	Lithium-Ion Batteries
SCs	Supercapacitors
SIBs	Sodium Ion batteries
PHEV	plug-in hybrid electric vehicles
ICE	Internal combustion engine
SnS	Tin Sulfide
ZnS	Zinc Sulfide
NiMH	Nickel metal hydride
g-C ₃ N ₄	Graphitic Carbon nitride
EC	Ethylene Carbonate
DMC	Dimethyl carbonate
EMC	Ethylene methyl carbonate
ESS	Energy Storage Systems
XRD	X-Ray Diffraction
SEM	Scanning Electron Microscope

SEM	Scanning Electron Microscope
XPS	X-Ray photoelectron Spectroscopy
FTIR	Fourier Transformation Infrared
CV	Cyclic Voltammetry
GCD	Galvanostatic Charge and Discharge
EIS	Electrochemical Impedance Spectroscopy

ABSTRACT

Multifunctional properties of ternary composites play an important role in fabricating high performance energy storage devices. This study explores the benefits of SnS:ZnS@g-C₃N₄ ternary composite in the development of lithium-ion batteries (LIBs). In this regard, SnS:ZnS@g-C₃N₄ composite is synthesized through facile solvothermal process with subsequent thermal treatments and investigated for LIBs. The porous nature and increased conductivity provide an opportunity to boost the lithium storage capabilities of SnS:ZnS@g-C₃N₄ composite. The anchoring of SnS:ZnS heterostructure on the graphitic carbon nitride (g-C₃N₄) exploits the synergistic effects between components to overcome the volume expansion occurs in anode material. It is found that the fabricated anode achieves a remarkable initial discharge capacity of 1623 mAhg⁻¹. Moreover, the electrode maintains a robust reversible capacity of 1045 mAhg⁻¹ at 0.3C over 800 cycles. In contrast, the pristine SnS:ZnS, SnS and ZnS anode shows exponential decline in specific capacity at 0.3C. In addition, the impedance measurements reveal that SnS:ZnS@g-C₃N₄ exhibits enhanced kinetics as compared to pristine SnS, ZnS, and SnS:ZnS. These findings highlight the superior electrochemical performance of SnS:ZnS@g-C₃N₄ as an anode material for lithium-ion batteries and offers a strategic pathway towards the development of advanced anode materials that addressing key challenges in the field of lithium-ion battery technology.

Keywords: Lithium-Ion Batteries, Tin Sulfide, Zinc Sulfide, Energy Storage, Metal Ion Batteries, Graphitic Carbon nitride.

CHAPTER 1: INTRODUCTION

1.1 Motivation

Energy is the greatest important constituent for the existence of humankind and plays a dynamic role in the evolution of human development. Nowadays, more than 80% of the world's energy comes from non-renewable energy-sources like fossil-fuels like coal, oil, and natural gas. When these fuels are burned, CO₂ is released, a primary contributor to climate change including the emission of other hazardous gases, an increased carbon footprint leads to negative impacts on nature, such as greenhouse effect, climate change, desertification, and the destruction of various plant and animal species.

Climate change and diminishing fossil fuels are pushing society towards renewables as a solution to it. With the increasing global energy consumption, clean energy has become more important. Many energy-storage devices, such as supercapacitors (Pseudo and Hybrid supercapacitors) and batteries, convert chemical energy directly into electrical energy and electrical energy to chemical and vice versa.

Fuel cells, which convert electrochemical energy directly into power, also offer practical solutions for a wide range of applications. These include electric-vehicles (EVs), move-able electronics, grid energy storage, and p applications in defense and space missions [1, 2].

A Ragone-plot (Figure 1.1) illustrates the comparative energy-density and power density working attributes of various energy-storage technologies. It demonstrates that capacitors are particularly proficient in high-power scenarios, whereas fuel cells are most effective for generating energy on a large scale. Li-ion Batteries positioned in the middle range of the spectrum, display performance features that lie between these two extremes.

This positioning renders them suitable for an extensive range of solicitations, such as powering moveable electronic devices and, significantly, for transportation purposes in both traditional internal-combustion engine (ICE) vehicles and electrical vehicles.

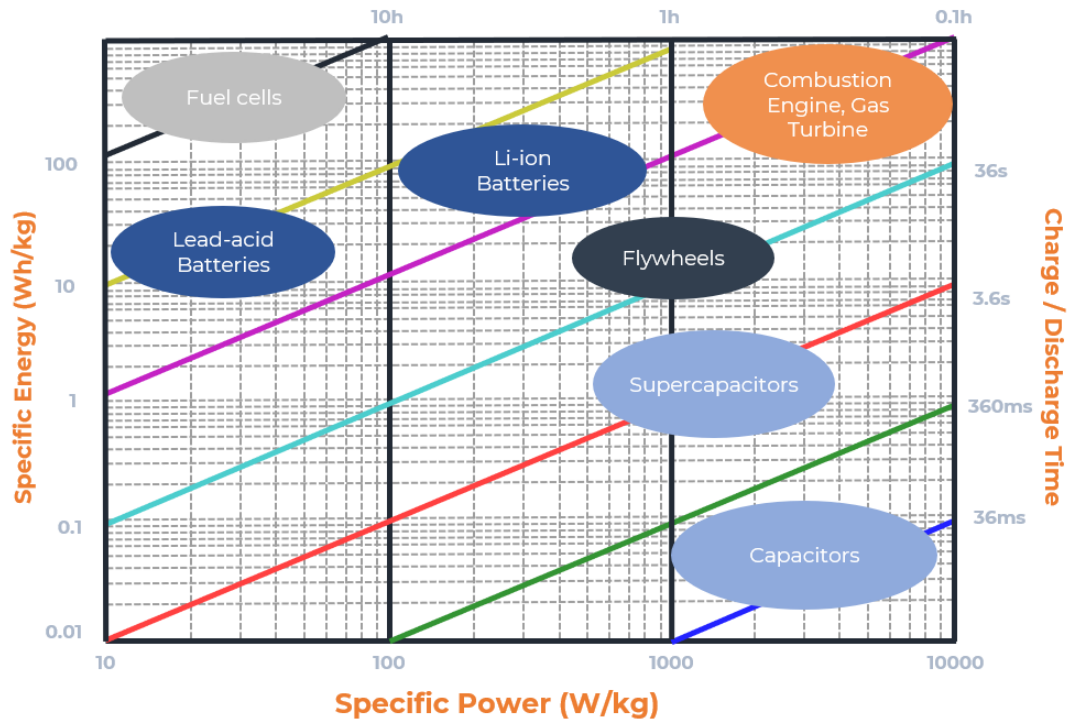


Figure 1.1: Ragone-plot showing the performance domain of various types electrochemical energy- storage devices compared to internal-combustion gas engine [3].

1.2 Background

Li-ion batteries have become essential for moveable energy-storage equipment's because of their high energy density and compact structure. They considered LIBs as the best form of battery systems established since Alessandro Volta invented the 1st battery in the early 19th century. LIBs was commercialized by Sony Corporation, for the first time, in 1990 with tremendous improvement from the conventional battery technology, started targeting the consumer electronics market like mobile phones, laptops, PDAs, digital cameras [4].

As LIBs engineering changes it's storage capacity, cycle life, stability, durability, and safety so have greatly extended the application from consumer electronics toeuteic tools, transportation largely in electrical vehicles, and plug-in hybrid electric vehicles (PHEV).

Because of progressive exhaustion of non-renewable energy forms added to the increasing emergence of worries regarding the detrimental effects of conventional energy-related technologies, the focus on renewable and sustainable energy storage systems has developed considerably [2]. The shift towards the range of environmentally friendly technologies is duly complemented by the increasing adoption of wearable electronics and hybrid electric vehicles that require advanced solutions to power them. LIBs, SIBs and SCs are vital technologies in electrochemical energy storage applied in numerous industries to fulfil different tasks [5].

1.2.1 Energy Storage Systems (ESS) Overview

Energy Storage Systems (ESS) are important components of modern energies infra-structure and are categorized into two main types indirect and direct storage which are further divided into the following devices.

1.2.2 Indirect Storage

- **Artificial Reservoirs:** Pumped hydroelectric storage facilities that use elevation differences to store and release energy.
- **Natural Reservoirs:** These include:
 - ✓ **Compressed Air Energy Storage (CAES):** Utilizes natural underground formations or tanks to store compressed air, which can be released to generate electricity.
 - ✓ **Hydropower:** Leverages natural water flows in rivers and dams to generate electricity.
 - ✓ **Thermal Energy Storage:** Stores heat energy, which can later be converted to electricity or used directly for heating.

• *1.2.3 Direct Storage*

- **Magnetic Energy Storage: (SMES)** Pump and stores electricity in a magneti- field produced by running DC through a superconductive coil.

- Electrical Storage: (Batteries, Supercapacitors)

1.2.4 Battery vs Supercapacitors

Supercapacitors and batteries are different in terms of the manner they store energy and in their functioning capabilities, although they have their merits, demerits, and applications. For instance, Li-ion batteries (LIBs) are mainly focused on energy storage by conversion through electrochemical reaction as energy is stored by the movement of lithium ions between positive and negative electrodes.

Great amount of energy-density can be achieved using this method, and thus it's appropriate to use it for long-term storage for uses such as electric cars and portable devices. However, this advantage comes with trade-offs, batteries are normally associated with low power density, and lower charge and discharge rates as well. Moreover, conversion-based energy storage take away the usable cycles of the battery and is lethal in some conditions, with faded capacity and thermal runaway [6, 7].

On the other side, supercapacitors occur as energy-storage equipment that store energy in an EDL at the surface of the electrode and the electrolyte. This method of energy storage permits extreme charge and discharge rates, which makes the supercapacitor attains high power-density than batteries. Therefore, supercapacitors are ideal where we find the energy density high enough, can be used like a regenerative breakage system or emergency power for gadgets.

Since the supercapacitors operate mechanically and rather than chemically, their cycle life is significantly longer and could be in the region of a million cycles before they start to degrade. However, supercapacitors are identified to offer low energy density which in essence does not allow the storage of large amounts of energy for long durations.

This makes them unsuitable for use in circumstances where high power is required continuously. So far energy storage being important in battery and supercapacitor technologies, it becomes evident that these technologies would require a future wherein rated energy materials as an integration of features of battery and supercapacitor will be more useful in different applications [8, 9].

1.3 Battery

In simple terms, a battery is an electro-chemical equipment that changes chemical energy into electrical energy via a Redox-reaction mechanism. This conversion occurs in one of the simplest entities forming an ‘electrochemical cell’. Nevertheless, a battery may be constituted of several cells joined in series to set up an electrical flow. As Li et al. (2020) REF? explain, batteries are typically composed of three main components: An electrode known as an anode, the other is known as a cathode and the material in between these two electrodes is called the electrolyte. As soon as the battery anode (-) and cathode (+) are connected to an external circuit the electrochemical process starts; this results in a chemical change of the electrolyte and the electrode. The reaction that occurs is used in moving positive ions from the -ve end to the +ve end through the electrolyte and vice versa, but the electrons are transferred from the anode through the external circuit to the cathode and generate electricity to power various appliances as indicated in Figure 1.2. This electron movement persists until the electrode cannot furnish any more of it, and this characterizes in simple terms the batteries as portable sources of electrical energy [10].

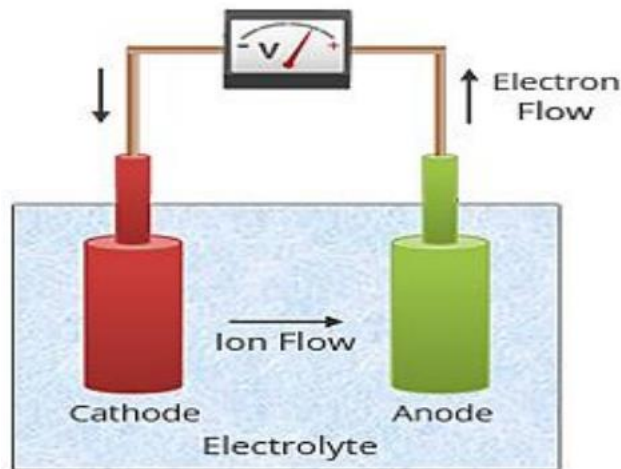


Figure 1.2: Simple Battery Setup.

The other component that is of so much significance in the functionality of a battery is the separator. It is situated in b/w the cathode and anode, and it is an ion conductor that keeps the electrodes separated to prevent the formation of a direct electrical connection the results in short-circuiting.

For such reasons and as explained the quality and type of the separator directly affect the life cycle, safety, energy-density, and power-density of a battery. Therefore, because of role of separator in enhancing the performance and in addition, the security of the battery, the separator occupies a significant position in the new generations of batteries.

It is due to such a complex of materials and processes that batteries manage to deliver energy in a variety of utilizations from miniature gadgets to utility-scale energy storage devices [11].

1.3.1 Primary Batteries Vs Secondary Batteries

Batteries are divided into 2 fundamental types: primary (non-rechargeable) and secondary (rechargeable). Non-rechargeable batteries are used once until they deplete their chemical ingredients and give one side discharging reaction after that disposed of. They are known for their simplicity and convenience but lack the capability for recycling and require minimal maintenance.

In contrast, rechargeable batteries can be recharged, reversible reactions, and again used many times, making them a more sustainable option over the long term as indicated below in Table 1.1 comparison of these battery types, including updated examples and characteristics.

Table 1.1: Comparison Between Primary and Secondary Batteries.

Characteristics	Primary Battery	Secondary Battery
Recharge-ability	Non-rechargeable	Rechargeable
Maintenance	Periodic maintenance	Low maintenance

Cost	Low	High
Cycle life	Short	Long
Toxic	Yes	Less
Examples	Lead acid	Li-Ion, Na-ion, Metal Air batteries, NiMH

Recent studies highlight the basic differences in the chemical setup and functional mechanisms between these battery types. Primary batteries, often referred to as dry cells, contain an electrolyte that is either embedded in a separator or held within an absorbent material. This setup restricts the free movement of ions, characteristic of liquid electrolytes found in secondary batteries. Alkaline batteries, a subset of primary batteries, utilize potassium hydroxide in a semi-solid form, which immobilizes the ions after their initial reaction, rendering the battery incapable of recharging once depleted [12].

Conversely, secondary batteries incorporate a freely flowing liquid electrolyte that permeates the internal structure of the cell, enhancing ion mobility which is crucial for repeated charging and discharging cycles. This setup not only allows for higher energy efficiency but also supports greater power output and lower viscosity, significantly improving overall battery performance. Technologies such as Li-ion and Ni-metal hydride (NiMH) exemplify this type, commonly used in applications demanding extensive reuse and higher power capacities, such as in electric vehicles and portable electronics [13]. Recent advancements have further refined secondary battery technologies, focusing on improving the life cycle, reducing charge times, and enhancing safety protocols to prevent issues like overheating and thermal runaway [14].

1.3.2 Lithium-Ion batteries (LIBs)

Li-ion batteries developed as the most prominent contenders in battery technology. The beneficial features of the Li-ion have established it as the preferred material currently, because of the presence of the Li/Li⁺ redox pair. Li has the lowest redox potential of -3.04

V compared to other elements in the electrochemical potential series as indicated in Figure 1.3. Additionally, Li is one of the lightest elements on the periodic table, with a molar mass of 6.94 g mol^{-1} [15]. Due to their low weight and the smallest -ve electrode potential of Lithium, LIBs have the high energy density compared to other straight battery systems. Due to these characteristics, LIBs are exceptionally required after for usage in moveable electrical devices and electric vehicles.

	Reduction Half-Reaction	E° (V)	
Stronger oxidizing agent ↑	$\text{F}_2(\text{g}) + 2 \text{e}^- \rightarrow 2 \text{F}^-(\text{aq})$	2.87	Weaker reducing agent ↓
	$\text{H}_2\text{O}_2(\text{aq}) + 2 \text{H}^+(\text{aq}) + 2 \text{e}^- \rightarrow 2 \text{H}_2\text{O}(\text{l})$	1.78	
	$\text{MnO}_4^-(\text{aq}) + 8 \text{H}^+(\text{aq}) + 5 \text{e}^- \rightarrow \text{Mn}^{2+}(\text{aq}) + 4 \text{H}_2\text{O}(\text{l})$	1.51	
	$\text{Cl}_2(\text{g}) + 2 \text{e}^- \rightarrow 2 \text{Cl}^-(\text{aq})$	1.36	
	$\text{Cr}_2\text{O}_7^{2-}(\text{aq}) + 14 \text{H}^+(\text{aq}) + 6 \text{e}^- \rightarrow 2 \text{Cr}^{3+}(\text{aq}) + 7 \text{H}_2\text{O}(\text{l})$	1.33	
	$\text{O}_2(\text{g}) + 4 \text{H}^+(\text{aq}) + 4 \text{e}^- \rightarrow 2 \text{H}_2\text{O}(\text{l})$	1.23	
	$\text{Br}_2(\text{aq}) + 2 \text{e}^- \rightarrow 2 \text{Br}^-(\text{aq})$	1.09	
	$\text{Ag}^+(\text{aq}) + \text{e}^- \rightarrow \text{Ag}(\text{s})$	0.80	
	$\text{Fe}^{3+}(\text{aq}) + \text{e}^- \rightarrow \text{Fe}^{2+}(\text{aq})$	0.77	
	$\text{O}_2(\text{g}) + 2 \text{H}^+(\text{aq}) + 2 \text{e}^- \rightarrow \text{H}_2\text{O}_2(\text{aq})$	0.70	
	$\text{I}_2(\text{s}) + 2 \text{e}^- \rightarrow 2 \text{I}^-(\text{aq})$	0.54	
	$\text{O}_2(\text{g}) + 2 \text{H}_2\text{O}(\text{l}) + 4 \text{e}^- \rightarrow 4 \text{OH}^-(\text{aq})$	0.40	
	$\text{Cu}^{2+}(\text{aq}) + 2 \text{e}^- \rightarrow \text{Cu}(\text{s})$	0.34	
	$\text{Sn}^{4+}(\text{aq}) + 2 \text{e}^- \rightarrow \text{Sn}^{2+}(\text{aq})$	0.15	
	$2 \text{H}^+(\text{aq}) + 2 \text{e}^- \rightarrow \text{H}_2(\text{g})$	0	
$\text{Pb}^{2+}(\text{aq}) + 2 \text{e}^- \rightarrow \text{Pb}(\text{s})$	-0.13		
$\text{Ni}^{2+}(\text{aq}) + 2 \text{e}^- \rightarrow \text{Ni}(\text{s})$	-0.26		
$\text{Cd}^{2+}(\text{aq}) + 2 \text{e}^- \rightarrow \text{Cd}(\text{s})$	-0.40		
$\text{Fe}^{2+}(\text{aq}) + 2 \text{e}^- \rightarrow \text{Fe}(\text{s})$	-0.45		
$\text{Zn}^{2+}(\text{aq}) + 2 \text{e}^- \rightarrow \text{Zn}(\text{s})$	-0.76		
$2 \text{H}_2\text{O}(\text{l}) + 2 \text{e}^- \rightarrow \text{H}_2(\text{g}) + 2 \text{OH}^-(\text{aq})$	-0.83		
$\text{Al}^{3+}(\text{aq}) + 3 \text{e}^- \rightarrow \text{Al}(\text{s})$	-1.66		
$\text{Mg}^{2+}(\text{aq}) + 2 \text{e}^- \rightarrow \text{Mg}(\text{s})$	-2.37		
$\text{Na}^+(\text{aq}) + \text{e}^- \rightarrow \text{Na}(\text{s})$	-2.71		
$\text{Li}^+(\text{aq}) + \text{e}^- \rightarrow \text{Li}(\text{s})$	-3.04		
Weaker oxidizing agent			Stronger reducing agent

Figure 1.3: Standard Reduction Potential of different elements at 25°C [16]

Sony was the first to commercially introduce LIBs in 1991. Batteries are indispensable for charging displays, sensors, RFID tags, solar cells, and portable devices, among other applications [17]. Lithium-ion batteries offers a distinctive blend of high power and energy densities in both weight-based (gravimetric) and volume-based (volumetric) measurements applied to moveable electronics systems, electronic textiles, medical diagnostics, and hybrid electric cars. Higher specific energy-densities are greatly desired for electronics and electron-mobility properties. The global market for lithium-ion batteries (LIBs) is mostly centered on energy storage in portable gadgets and electric vehicles. It is projected to have a significant rise of over \$76 billion in 2020 [18, 19]. The rate performance and specific capacitance of Li-ion batteries are contingent upon their structure and exhibit significant variation among different manufacturers.

An outstanding benefit of Li-ion batteries is their extended lifespan and their capacity to operate effectively in fluctuating temperatures. For instance, lithium-ion batteries show exceptional stability even after undergoing 500 cycles, which is significantly higher compared to other similar alternatives (nickel-cadmium and nickel metal hydride). Cyclability refers to the capacity of a battery to endure a specific number of charging cycles throughout its lifespan. The primary safety issue related to lithium-ion batteries is the risk of overheating or overcharging, which can lead to thermal runaway and cell rupture. This technique has significant limitations, which are its biggest destruct when compared to other battery technologies. There have been numerous instances of cell phones and laptops explosion, causing significant losses. Around 80 percent of recent research publications on Lithium-ion batteries have mostly gave overcharging, safety measures, as well as internal short-circuits, and the impact of varied operating temperatures [20].

1.3.3 History of Li-Ion batteries (LIBs)

Lithium possesses the highest electrochemical potential and offers the biggest energy density compared to other metals and is the least heavy of all metals. In 1912, G.N Lewis pioneered the startling process of harnessing the true capabilities of Li-ion, the dean of the chemistry department at the University of California, Berkeley. The first easily accessible lithium-ion non-rechargeable batteries were not launched until the early 1970s. This innovation was proposed by M.S. Whittingham at Exxon [21]. The batteries were manufactured using Li metal as the +ve and TiS_2 as the -ve. Although the positive cathode responded appropriately, the lithium metal anode exhibited aberrant dendrite growth during cycling [22].

In the 1980s, efforts were made to develop rechargeable lithium batteries. It came to light that these batteries can deliver both high voltage and impressive capacity which utilize a lithium metal anode. These traits culminated in an exceptionally elevated level of energy. In 2019, 3 scientists were awarded the Nobel Prize in Chemistry for their pioneering advancements in LIBs as indicated below in Figure 1.3.

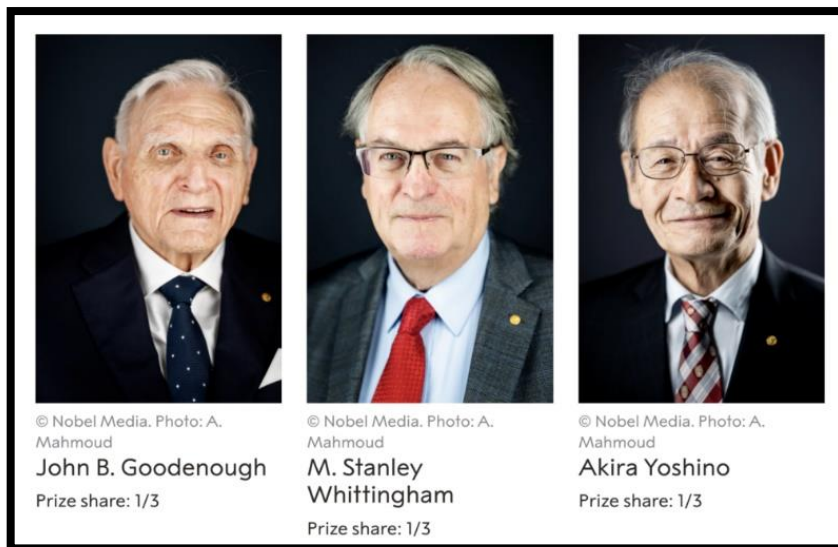


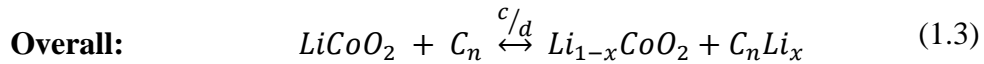
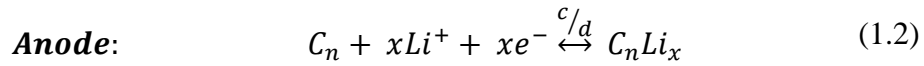
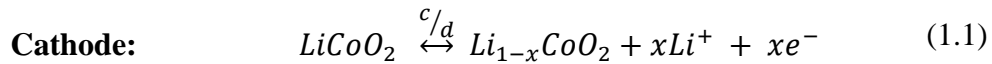
Figure 1.4: Nobel laureate in Chemistry (Li-Ion batteries) [23].

Attempts to increase the density were unsuccessful because of safety concerns arising from the violent chemical reactions triggered by fluctuations in temperature. Consequently, the focus of research turned to non-metallic lithium batteries that utilize lithium-ions, which are relatively safer than Li-metal. A breakthrough in the progress of Li-batteries arose when intercalation materials were discovered, allowing for the use of lithium as an insertion material in rechargeable-batteries. Rachid Yazami et al. demonstrated the electrochemical characteristics of lithium intercalation in graphite in 1986. Akira Yoshino developed the first LCO cathode with coke anode in 1991 also in the same year Sony company established the first commercial Li-ion battery, which was engineered by John Goodenough's research team [24, 25].

1.3.4 Why Rocking Chair batteries?

Li-ion battery is currently the finest prominent type of battery. The operation concept is formed on the intercalation/insertion electrochemistry of Li-ions into a host material. Lithium ions can intermix with various materials at varying electrochemical potentials. By selecting two distinct materials with a significant voltage disparity, it becomes possible to store Li^+ ions at two distinct energy levels.

This phenomenon also elucidates the underlying principle of energy storage. The process of charging or discharging requires the transport of Li^+ ions between the 2 electrodes, to the movement of a rocking chair, to store or withdraw energy from the battery. Commercial batteries commonly use graphite as the anodic material due to its ability to provide lesser voltage levels to the Li^+ ions. LiCoO_2 based compounds are commonly selected as the cathode material in most LIBs [26]. The anodic half-cell reaction can be explained as follows:



Lithium carbide (LiC_6) reacts with carbon dioxide (CO_2) to form graphite (C_6) and lithium carbonate (Li_2CO_3).

When the voltage differentiation b/w the +ve and -ve exceeds the electrochemical stability range of aqueous electrolytes, it is necessary to use alternative organic electrolytes. These electrolytes help maintain voltages over 5 V.

Electrolytes primarily blends of carbonate solvents, including dimethyl carbonate (DMC), ethylene carbonate (EC), propylene carbonate (PC), and others. Once again, the 2 electrodes are kept apart by an ion conducting membrane also called separator, which serves the purpose of preventing an electrical short circuit between the two electrodes. Rocking chair batteries can be utilized in several electrochemical processes, not limited to monovalent alkali metal ions, but also involving bivalent and even trivalent ions.

Each of these concepts is associated with its own set of obstacles, benefits, and limitations. In addition, li ion batteries has long cycle life, high energy density, high operating voltage 3.6 as compared to primary batteries moreover its act as more reducing

agent that has the potential to give off more electron than other metals easily, which is necessarily for redox reaction in a cell, as demonstrated in the below **Table 1.2**.

Table 1.2: Performance comparison of different batteries.

Characteristics	Lead-Acid	Ni-Cd	Ni-MH	Li-Ion
Cell Voltage	2	1.2	1.2	3.7
Specific energy (Wh/kg)	1-60	20-55	1-80	3-150
Specific power (W/kg)	< 300	150-300	< 200	100-1000
Energy density (kWh/m ³)	25-60	25	70-100	80-200
Power density (MW/ m ³)	< 0.6	0.125	1.5-4	0.4-2
Maximum cycles	200-700	500-1000	600-1000	3000
Cost (\$/kWh)	125	600	540	600
Cost (\$/kW)	200	600	100	1100
Efficiency (%)	75-90	75	81	99

1.3.5 Applications of Li-ion batteries

- Portable Electronics:
 - ✓ Powers smartphones, laptops, and digital cameras.
 - ✓ Ensures extended usage and quick recharges.

- Electric Vehicles (EVs):
 - ✓ Core technology in electric cars and buses.
 - ✓ Offers high energy density and efficiency.
- Energy Storage Systems:
 - ✓ Stores solar and wind energy in residential and commercial settings.
 - ✓ Enhances grid stability and energy security.
- Medical Devices:
 - ✓ Operates portable oxygen machines and wheelchairs.
 - ✓ Provides reliable power for critical healthcare equipment.
- Uninterruptible Power Supplies (UPS):
 - ✓ Critical for continuity in data centers, hospitals, and communication networks.
 - ✓ Provides backup during power failures.
- Aerospace Applications:
 - ✓ Used in satellites, spacecraft, and drones.
 - ✓ Ensures reliability in extreme environmental conditions.
- Wearable Technology:
 - ✓ Fuels the expanding market of smartwatches and fitness trackers.
 - ✓ Supports advanced features with prolonged battery life.
- Marine Applications:

- ✓ Powers electric and hybrid boats.
- ✓ Offers a cleaner alternative to gasoline engines.
- Recreational Vehicles (RVs):
 - ✓ Ideal for off-grid traveling, powering appliances and systems in RVs.
 - ✓ Provides high capacity and quick recharge benefits.
- Robotics:
 - ✓ Powers industrial and personal robots.
 - ✓ Ensures longer operation and reliable autonomy [27]

1.3.6 Working Principle of Li-ion batteries

A Lithium-ion battery that stores energy chemically through redox processes is a type of secondary battery. This can be accomplished by using li-intercalation and the positive (cathode) and negative (anode) electrodes. Undergoes charging and discharging, are commonly known as "Rocking-chair" batteries, so li-ions oscillate between the cathode and the anode [28]. The Li-ion battery consists of these main components:

- Anode
- Cathode
- Separator
- Electrolyte

These components can be made from numerous substances. The cathode serves as a positively charged electrode. The cathode takes electrons and endures reduction, yet the anode serves as a negative electrode, donating electrons and undergoing oxidation during the discharge cycles. The electrodes remain physically detached from one other, but they are electrically linked across the electrolyte. Meanwhile, the separating membrane helps

to prevent any contact b/w the electrodes, while nevertheless permitting the passage of ions [30]. During charging Li ions towards anode material through the electrolyte which is ionically conductor and electron from the outer circuit. While during the charging process, lithium ions travel from the positive to the negative and electrons are extracted from the positive end through an external-field and subsequently transferred to the negative side shown in Figure 1.5.

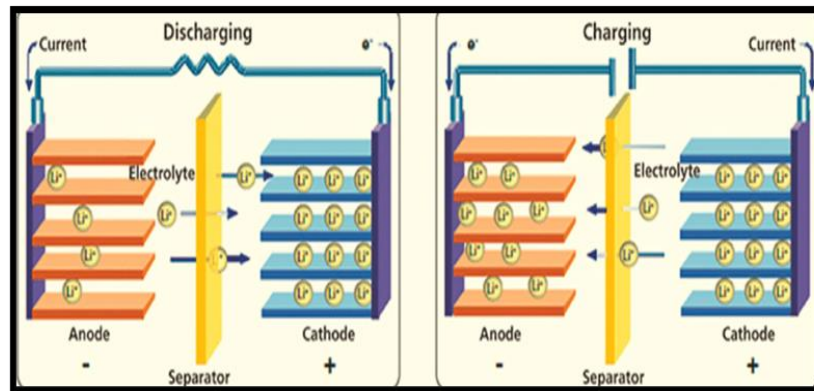


Figure 1.5: Charge and Discharge Phenomena of Lithium ion Batteries [29]

In the above circuit, ions are fed into the cathode while electrons from an external circuit are used to neutralize the charge. An electrode often includes conductive carbon and a polymer binder. The binder is an essential aspect of the electrode material. This tightly attaches the active substance to the current collectors. Therefore, the adhesive capacity of the binder is crucial for preserving the strength of the electrode matrix [31]. The working of a battery is generally determined by the characteristics of its anode, cathode, and electrolyte. The cathode is a particularly promising topic for investigation due to its high free energy of reaction with lithium.

1.3.7 Material attributes

There are four main parts of Li ion cell anode, cathode, electrolyte and separator must be selected depending on the battery functional needs:

1.3.8 Anode

Generally, negative electrode is made up of carbonaceous material graphite which is commercialized and widely utilized as a major material for the anode. The fundamental constraints of elemental lithium include the production of needle-like dendrites that penetrate the separator, leading to the occurrence of short circuits in the entire cell. The anode is an essential aspect of the rechargeable battery and, depending on its characteristics and shape, it greatly influences the performance of the battery. Currently, graphite is utilized extensively as the basic material for anodes in most commercially accessible products for its distinctive hierarchical structure. However, graphite anode material is giving low capacity 372 mAhg^{-1} and high internal resistance which leads towards low energy density batteries so now researchers are trying to explore new material like Si, Sn, and Titanium to overcome the issue associated with conventional graphite [32].

1.3.9 Cathode

The cathodes must contain two important characteristics in that they must contain an open crystal structure to accommodate Li-ion and at the same time should be able to accommodate compensation electrons moving from the anode. Thus, many times used cathodes in the Li-ion batteries are metal oxides which contain transition metals such as layered LiCoO_2 , polyanion materials including $\text{Li}_2\text{FePO}_4\text{F}$, LiMn_2O_4 , $\text{LiCo}_{1/3}\text{Ni}_{1/3}\text{Mn}_{1/3}\text{O}_2$ and LiNiO_2 with different crystal structures [33].

1.3.10 Electrolyte

Various forms of electrolytes exist, notably liquid electrolytes, solid electrolytes, and gel electrolytes. Liquid electrolytes are the dominant type of electrolytes used within the field of rechargeable batteries.

Due to high flammability of lithium and its high reactivity with water, the electrolyte employed in Lithium salts of organic anions are often used for the electrolyte of batteries and are normally nonaqueous. This dangerous reaction must not occur to eliminate the risk of explosion in the battery.

Moreover, the non-aqueous electrolyte which is used ideally must possess good conductance and this forms the most conspicuous requirement. In general, an electrolyte solution containing salts and other components is ideally suited for use in the disclosed process to which a grade solvent of 25 mS cm^{-1} conductivity must be added at ambient temperature.

LiPF_6 is lithium salt that is often mixed in organic solvents such as e. g. dimethyl carbonate (DMC), ethyl methyl carbonate (EMC) and ethylene carbonate (EC) [34].

1.3.11 Separator

The separator plays an important role in the overall performance of the battery. The sheet is made of microporous polyethylene & polypropylene, and it can be either mono or multilayer. Its purpose is to isolate both electrodes. Consequently, it necessarily contains the following individualities:

- High mechanical-strength to avoid electrical contact between the electrodes.
- Low electrical conductivity.
- The separator possesses excellent wettability, enabling it to absorb electrolytes and achieve high ionic conductivity.
- The battery must exhibit chemical inertness towards the other elements of the battery, meaning it should not undergo any reaction with the various parts of the battery.

Certain separators actively contribute to cell safety by exhibiting ion impermeability at specific temperatures, hence preventing chemical reactions during thermal runaway.

The separators are referred to as "shutdown separators" and it is important to emphasize that this phenomenon is irreversible [35].

1.4 Limitations of Li-ion batteries

Though characterized by remarkable features, the application of (Li-ion) batteries in portable power have some problems. These limitations shall and should be considered, especially considering their overall applicability across different applications.

1.4.1 *Low Power Density*

Li-ion batteries allow a lot of energy to be stored and as such can be used broadly across multiple devices. But they lack reliability when it comes to the provision of power of immediate demand. This is because in applications that require short bursts of power such as electric cars that need a burst of acceleration, the battery flattens quickly, so there is constant cycling of charging and discharging. To overcome this, supplementary systems are used to control power output, but these new systems serve to raise both system complexity and cost [36].

1.4.2 *Safety Concerns / Explosive*

A significant concern has been made to safety since Lithium-ion batteries are made of flammable materials. Depending on the conditions such as overheating, shock or overcharging the life of such battery can go up in flames called thermal runaway. This may at times result in physical flames, or in extreme cases, explosions which are very dangerous.

These risks have been addressed in different ways by manufacturers through enhanced voltage regulators, but these measures tend to increase the battery's weight and its cost apart from perhaps making it less suitable for use in some incidences [37].

1.4.3 *Cost*

Li-ion batteries can also be expensive to purchase which is a limitation to their usage. One of the most significant drawbacks of EVs is that they are considerably expensive, and this high cost is attributed to the costly materials that are used in their manufacture and which include lithium, cobalt, and nickel [38].

Additionally, the production process of entry level smartphones is elaborate because accurate work and quality assurance are crucial in manufacturing this item, and

such works increase the cost of production. Therefore, the Li-ion batteries are relatively costly in contrast to other types of energy storage systems, which represents a major disadvantage regarding costs, especially when it comes to the application of energy storage in the consumer electronics market or large-scale energy storage stationary applications [35].

1.4.4 Temperature Window

Li-ion batteries perform best when they are operated within a certain temperature window. However, exposure to extreme temperatures has been known to bring out the worst in their performance level [39]. Cold can have a negative impact on the battery mainly because the efficiency and the capability of chemical reactions within the battery will be reduced.

On the contrary, high temperatures are damaging to batteries and can cause the decay of battery's materials, thus reducing the battery's cycle life and leading to thermal runaway [40]. This gives Li-ion batteries the drawback that they are not so effective in an environment where temperature fluctuations are extreme.

1.4.5 Supply and demand

Materials used in construction of Li-ion batteries, especially lithium and cobalt, are mainly sourced from a few geographical locations globally. This can cause a concentration of supply in one region, which can make it very sensitive to such conditions as geopolitics and trade barriers or restrictions.

Thus, these supply chain issues may result in constraints of Li-ion batteries, accelerate their cost, and therefore reduce access to such technologies like electric vehicles and renewable power plants [41].

1.4.6 Aging and Performance Degradation

As with any other battery, Li-ion batteries deteriorate gradually. The problem arises when Li-ion batteries are fully charged or over- discharged. . Every charge and discharge cycle results in loss of battery charge holding capacity and consequent discharge of battery power.

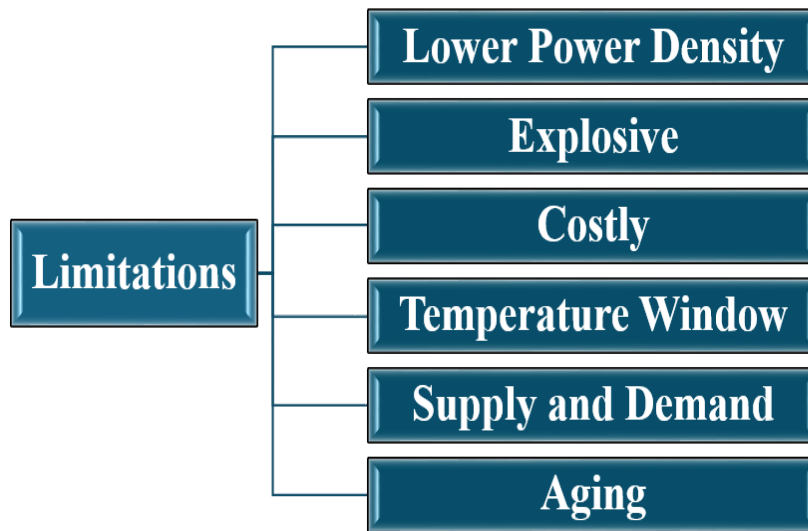


Figure 1.6: Flow Chart Diagram of Limitations of Li-Ion Batteries.

This ageing process will reduce the run times and at some point, the battery will be exhausted and replaced [42]. In specific uses such as electric cars, this degradation process can be very disadvantageous, and therefore may lead to increased overall cost and maintenance of the batteries. Also, the older batteries have low reliability, which can sometimes lead to failure; thereby increasing safety issues.

1.5 What is SnS?

Tin Sulfide SnS is a material made of tin (Sn) and with chalcogen group element sulfur (S) with promising future in the battery technology in terms of anode material. As a layered structure metal chalcogenides p-type semiconductor, SnS has the divalent tin oxidation states which are essential in the battery systems. This compound has a band-gap of approximately 1.3 eV, and its band gap was well suited to charge transfer processes important in energy storage applications. Notably, SnS has been characterized for high reversible theoretical capacity of 755 mAhg^{-1} and good electrical conductivity that are apparent to charge storage and high-rate capability of batteries. It can be alloyed and converted therefore considered for use in next generation Li ion and Na-ion batteries. These characteristics of properties make SnS lively and enable the growth of energy technology with better efficiency and sustainability [43].

Table 1.3: Chemical and Electrical Properties of SnS

Property	Description
Chemical composition	Tin (Sn), Sulfur (S), SnS
Crystal Structure	Orthorhombic
Bandgap	1.3 eV
Density	5.22 g/cm ³
Molar Mass	150.775 g/mol
Melting point	882 C (1,620 F; 1,155 K)
Bandgap type	Indirect

1.5.1 Structure of SnS

SnS has orthorhombic structure and can be described in terms of the layered layout of tin (gray) and Sulfide (yellow). Individual Tin atom is held by three S atoms in the same plane and one S atom from the adjacent plane forming a distorted octahedral coordination. This arrangement makes complexes of connected zigzag bonds of Sn and S along the b-axis.

The SnS layers align in the c-direction and relate to van der Waals forces that allow layer shift which leads to relatively large mechanical flexibility of the material. On the other hand, in the ab plane it is quite different, it is well bounded by strong covalent bonds which provides structural integrity. The weak interlayer forces along the c-axis allow for unique properties such as anisotropic electrical conductivity.

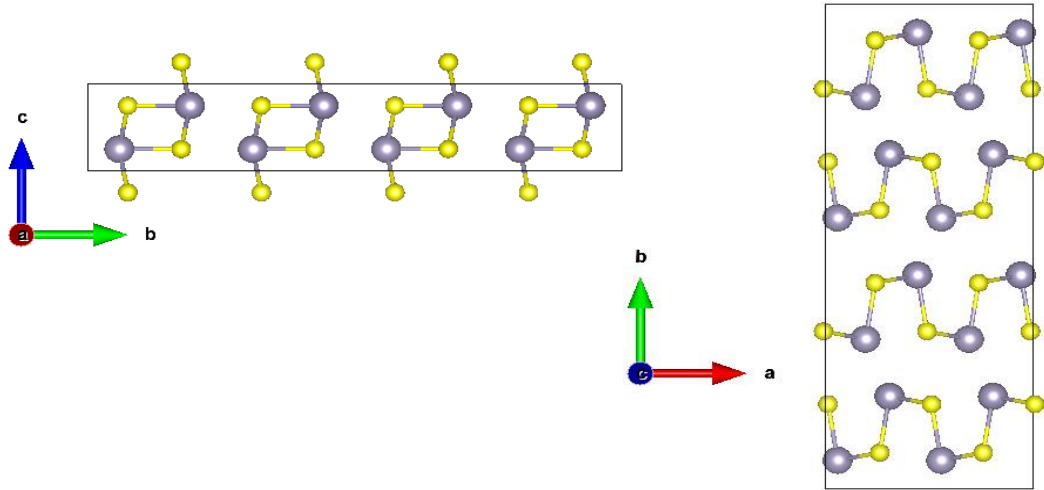


Figure 1.7: Orthorhombic Structure of SnS.

1.5.2 Advantages of SnS

- SnS has constituents that are nontoxic and easy to obtain, which therefore means that SnS is an inexpensive material to use in different fields.
- It is in this capacity that SnS can provide high theoretical capacity value to energy storage.
- Due to the direct bandgap of SnS, it is acknowledged as 1 of the best materials for opto-electronic gadget allowing effective usage of light in solar cells, light sources, and sensors.

1.5.3 Disadvantages of SnS

- SnS has been found to be sensitive to the deteriorating environments for instance when subjected to moisture or oxidative conditions, SnS has high instability which degrades its performance in the long run.
- In energy storage applications, SnS cycling stability can be still a problem that leads to SnS poor capacity fading over time.

1.6 What is ZnS?

Zinc sulfide (ZnS) is an inorganic compound composed of zinc (Zn) and sulfur (S) of which has been reported to be one of the anode-materials in batteries. Since it is a binary II-VI semiconductor, the bandgap of ZnS is about 3.6 to 3.9 eV which is quite suitable for charge transfer process especially in applications of energy storage devices. ZnS has theoretical capacity is 962 mAhg^{-1} and studied in electron mobility to electrical conductivity that describes its applicability to high-rate capability and charge storage in battery systems. It can also be integrated and altered if needed, thus suitable for use in the next generation Li-ion and Na-ion batteries. Such qualities of ZnS reduce energy storage times; therefore, improve the rate of development of energy storage systems [44].

Table 1.4: Chemical and Electrical Properties of ZnS

Property	Description
Chemical composition	Zinc (Zn), Sulfur (S), ZnS
Crystal Structure	Cubic
Bandgap	~3.7 eV
Density	4.09 g/cm^3
Molar Mass	97.46 g/mol
Melting point	1,850 °C (3,360 °F; 2,120 K)
Bandgap type	Direct

1.6.1 Structure of ZnS

ZnS crystallizes in cubic lattice system adopting the zinc blende structure. This structure is highly symmetric in which Zn atoms (grey) are surrounded by four S atoms (yellow) in a tetrahedral geometry. In the present coordination, every Zn atom has its coordination site occupied by four S atoms and vice-versa, thereby establishing strict coordination network of three-dimensional nature involving Zn-S linkages which are quite rigid and stable.

The tetrahedral coordination in the ZnS lattice makes the Zn-S bond distributed all over the lattice uniformly. This even distribution helps in imparting mechanical strengths and stability of the material. These coordination patterns are uniform in all the three crystallographic directions namely 'a', 'b' and 'c' as shown in the Figure (1.8).

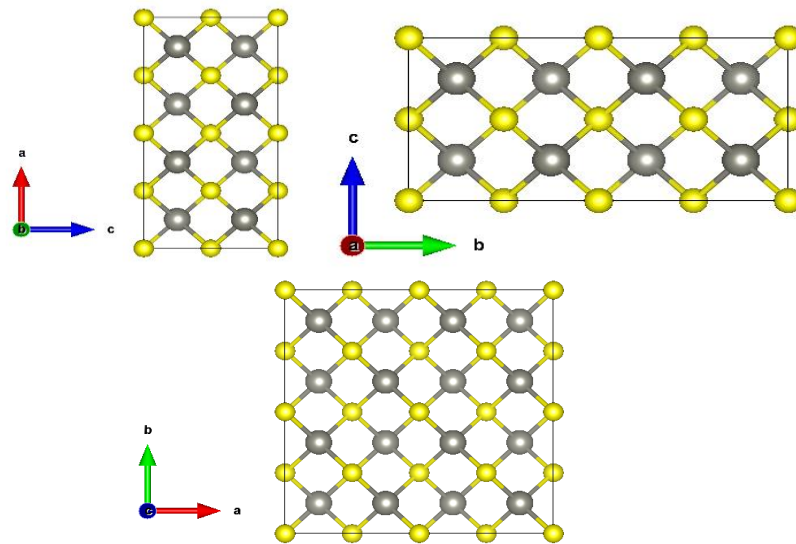


Figure 1.8: Cubic Structure of SnS

1.6.2 Lattice Orientation

- Top View (beside the c-axis): The sight at the top of the figure presents the Zn and S atoms disposed in diamond-like manner at the same levels, which is typical for the zinc blende structure.
- Side Views (along the a- and b-axes): Such views stress the highly symmetrical tetrahedral covalent bonding; this follows the isotropic

character of the material where the material's properties are also found to be equally distributed in all directions within the crystal lattice.

1.6.3 Advantages of ZnS

- The ZnS has a large bandgap, and hence it is commonly used in optoelectronics devices like UV LEDs and photodetector. This wide bandgap makes it possible for ZnS to be used in high energy optical applications.
- ZnS has high transparency in the visible region hence it is widely used in making lenses and windows in optical instruments.
- Due to the powerful tetrahedral covalent bond within the cubic lattice, mechanical properties of the material show some resilience with ZnS material utilized in a broad range of uses.

1.6.4 2 Disadvantages of ZnS

- ZnS has an absolute advantage in mechanical characteristics, but it is a brittle material, which complicates its use in the conditions where highly flexible material is needed.
- ZnS, in some instances, is rather unstable upon exposure to certain conditions such as moisture, which may slightly reduce the stability in some applications.

1.7 Significance and Research Objectives

The basic objective of this research is to evaluate the performance of SnS:ZnS@g-C₃N₄ nanocomposite for lithium-ion batteries. As batteries become more prevalent and gain attention, still consider emerging technologies that need more work to address their drawbacks. Because batteries require a lot of protection and are expensive, researchers have been pushed to employ a variety of innovative materials such as electrodes in them. This point of view claims that the study is important since it provides novel data on

whether the integration of SnS:ZnS@g-C₃N₄ composite mitigates the volume expansion and enhance the cyclic rate-performance of Li-ion batteries.

1.8 Research Objectives

1. Synthesizing the SnS:ZnS@g-C₃N₄ electrode material using solvothermal method.
2. Characterization of the synthesized SnS:ZnS@g-C₃N₄ material.

Fabrication and Testing of coin cell of SnS, ZnS, SnS:ZnS and SnS:ZnS@g-C₃N₄ as anode material for lithium-ion batteries

CHAPTER 2: LITERATURE REVIEW

2.1 Historical Background

Up to now carbonaceous material is used as anode material in commercial Li-ion batteries with high specific-capacity, long life-span and good cyclic efficiency but potential Li-ion batteries in electric automobiles requires higher energy-density and power-density. The presentation of LIBs depends on thermal history and structural morphology of carbon material. Today, the cathode in the market for LIBs typically consists of lithium materials like NCA, LiFePO_4 and NCM gaining attention due to their stable structure and long cycle life with counter electrode as graphite.

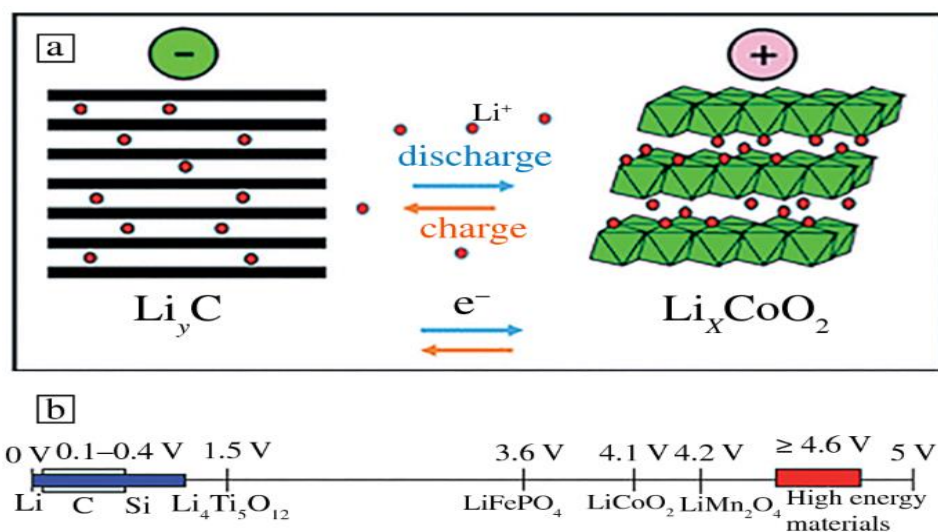


Figure 2.1: Graphite battery mechanism

In these graphite anodes, Li-ions are intercalated and de-intercalated in anode layers during the charge and discharge cyclic processes, resulting in the formation of graphite interpolate compounds. For the 1st time lithium-ion battery, developed by Yoshino, employed a carbon based anode (positive side), a LiCoO_2 cathode (negative side) as in Figure 2.1. Yet, the graphite anode's specific capacity is relatively modest at about 372 mAhg^{-1} , which is a bottleneck for satisfying the growing needs for higher energy density in LIBs. This necessitates the growth of new anode material to fulfill the demands for

higher energy densities at reasonable costs, ensuring sustainable energy storage and distribution. In this quest, transition metal chalcogenides (TMCs), particularly SnS and ZnS, are notable for their higher specific-capacities as 755 mAhg^{-1} and 962 mAhg^{-1} respectively with enhanced charging and discharging efficiencies in next-generation LIBs [45].

2.2 Common Anode Materials for Lithium-Ion Batteries

Efficacy of Li-ion batteries is greatly determined by the choice of anode materials, which are primarily categorized into three types. These categories define the electrochemical behavior and performance characteristics of the batteries. A detailed understanding of each type helps in optimizing battery design for specific applications, enhancing electrochemical performance, capacity, stability, energy density [46]. These types of anode materials with specific capacity distribution are shown in Figure 2.2.

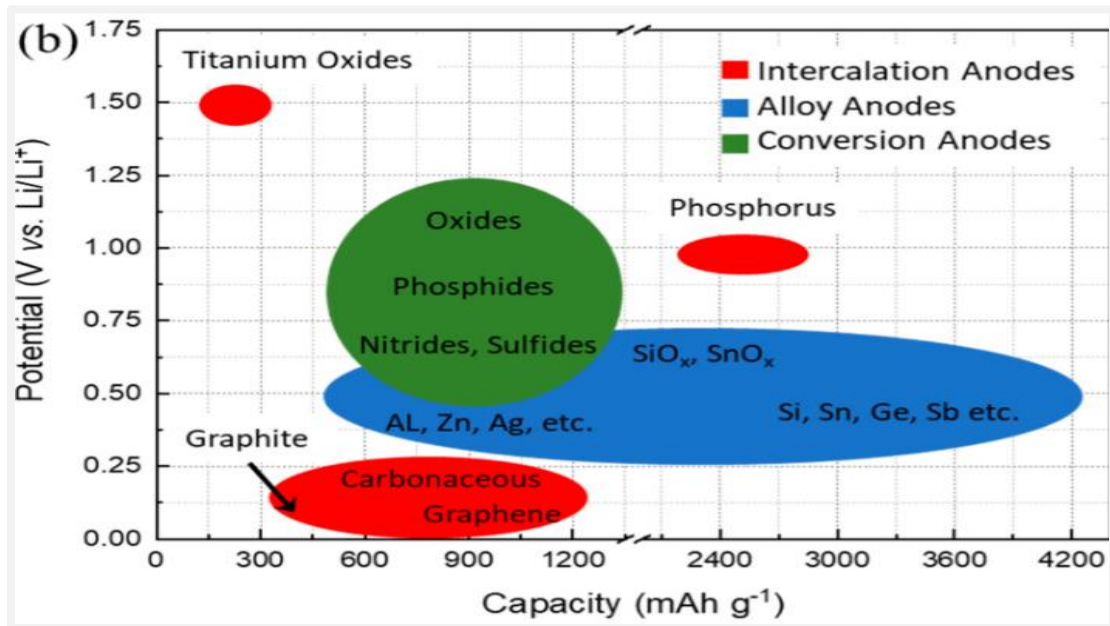


Figure 2.2: Specific Capacity and Operating Voltage of Various Anode [47].

2.2.1 Requirements of Anode Material

The ideal anode material for LIBs must have several characteristics:

- ✓ High specific capacity

- ✓ Excellent cycle life
- ✓ Higher kinetics (Fast charge and discharge capabilities)
- ✓ Low cost and easily available
- ✓ Environmental-friendly, non-toxic
- ✓ Low reaction against electrolyte during battery operational safety

2.2.2 Commercialized anode: Graphite, Hard Carbons

Understanding these requirements guides the selection and development of anode materials and drives innovations aimed at overcoming the limitations of current technologies [48]. The following sections will delve into how different classes of anode materials meet these diverse requirements, considering their inherent properties and potential for enhancements.

2.2.3 Intercalation Types

Graphite and Titanium Oxides are two intercalation types of anode material for LIBs. Graphite, known for its stability and long life, holds about 372 mAhg^{-1} capacity. It operates at potentials very close to lithium, minimizing the risk of lithium plating and enhancing safety (51).

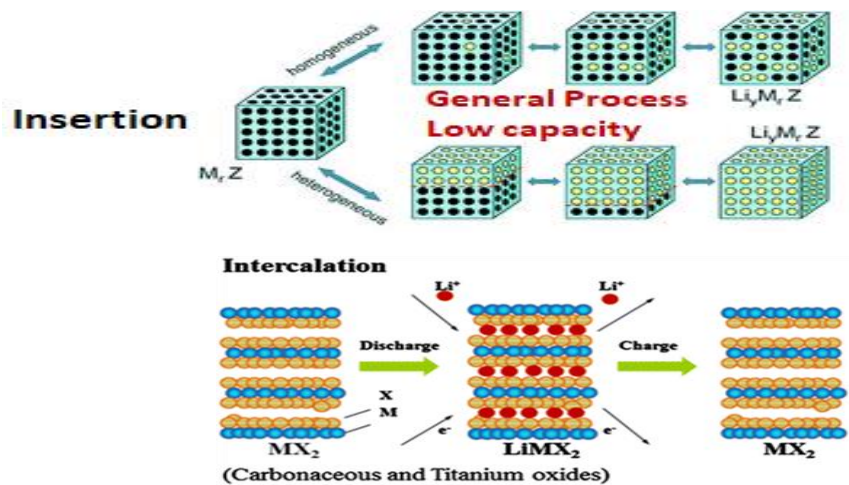


Figure 2.3: Mechanism of Intercalation Type Anode Material [49].

Titanium oxides, although offering lower capacities, operate at higher potentials, significantly reducing safety risks associated with electrode material degradation. (52) Transition Metal Chalcogenides (TMCs) offer promising alternatives with their unique properties such as high stability and capacity, suitable for high-energy applications (53). Lithium titanate (LTO) is another advanced material that provides excellent rate capabilities and cycle life and intercalations mechanism shown Figure 2.3 which making it ideal for automotive applications where quick charging is essential [50, 51].

2.2.4 Conversion Types

Metal oxides as (V_2O_5 , CuO, ZnO, WO_3 , Bi_2O_3 , Co_3O_4 , CoO, Fe_3O_4), Phosphides (NiP, FeP) and Nitrides (TiN , Si_3N_4) are conversion type class of anode material. These materials engage in conversion reactions when Li ion combine with metal that produce new lithium compounds, offering high capacities but encounter numerous challenges, such as poor cycling stability resulting from significant volume changes during charge-discharge cycles, inherently low electrical conductance, and the development of unstable solid electrolyte interface (SEI) that thickens with each cycle, consuming electrolyte and active lithium ions [52].

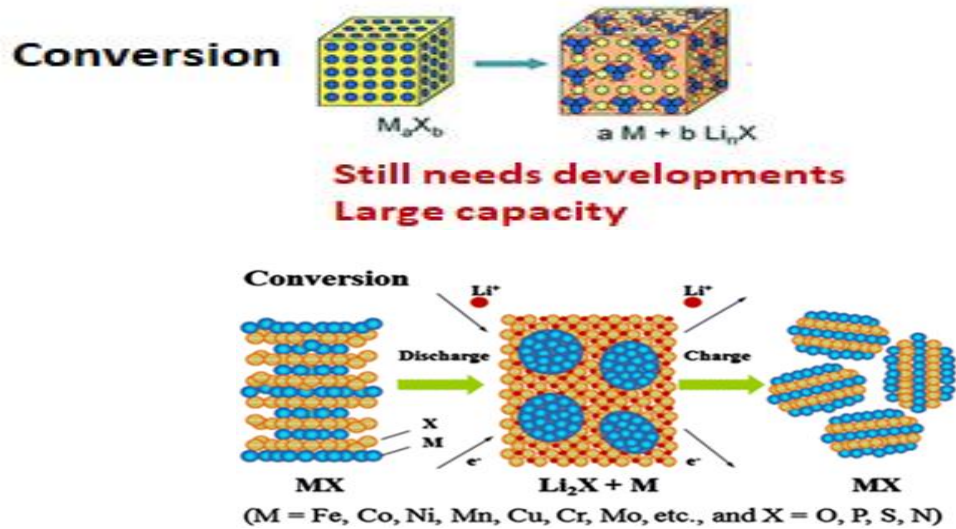


Figure 2.4: Mechanism of Conversion Type Anode Material [49].

Figure 2.4 indicating conversion reaction take place during the charging process and complications include the irreversible nature of some conversion reactions and

problematic thermal behaviors that heighten the risk of thermal runaway. These factors collectively degrade the battery's lifespan, efficiency, and safety, necessitating advanced solutions to mitigate these issues [53].

2.2.5 Alloy Types

Si, Sn, Ge, and Sb are promising alloy type anode material for lithium-ion batteries. Through them silicon offers the maximum theoretical capacity (up to 4200 mAhg^{-1}). Alloy-type anode materials are valued for their high theoretical capacities but are suffering from volume-expansion through lithium insertion process shown in below Figure 2.5, So volume expansions lead to stress generations and mechanical degradation which reduced battery cycle life. To mitigate these issues, recent advancements include nano structuring and the development of nanocomposite materials. Nano structuring involves reducing the particle size to mitigate the expansion and contraction more effectively during battery operation, while composite approaches integrate these alloys with carbonaceous material to buffer the volume changes and enhance electrical conductivity with alloy type anode material [54].

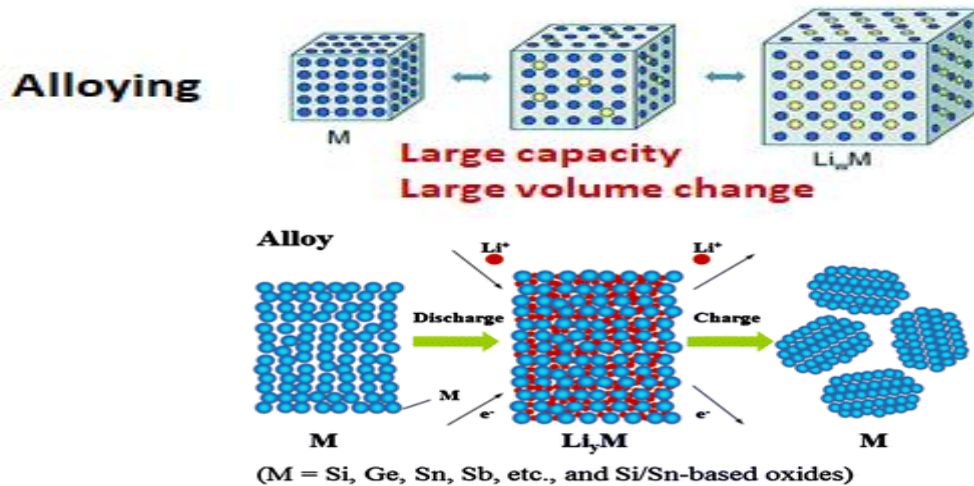


Figure 2.5: Mechanism of Alloy Type Anode Material [49].

These innovations aim to improve structural stability and enhance overall battery performance, offering promising directions for future battery technologies [55].

2.3 Why SnS and ZnS as an Electrode Material

2.3.1 High Theoretical Capacity and Energy Density

SnS stands out with an extraordinary theoretical capacity of about 645 mAhg⁻¹, which grants to a higher energy density, making it suitable for more energy-demanding applications. This capacity is significantly higher than traditional graphite anodes, enabling longer-lasting batteries or the potential for smaller, more compact battery designs. ZnS, while having a lower capacity, complements its application with good stability, offering a balanced choice for energy storage where safety and longevity are priorities [32].

2.3.2 Volume Expansion

SnS and ZnS both exhibit lower volume expansion contrasted to other high-capacity anodic materials like silicon (Si). This characteristic is crucial as it reduces mechanical stress within the battery during charging and discharging cycles, thus enhancing durability and longevity of the battery. SnS shows manageable expansion, while ZnS demonstrates even lower expansion rates, which helps sustain the structural reliability of the anode over numerous cycles [56].

2.3.3 Cost and Abundance

The cost-effectiveness of SnS and ZnS is derived from their composition of abundant, less expensive elements compared to rarer materials like cobalt and nickel. This not only makes them more affordable but also eases the supply chain constraints, supporting sustainable scaling of battery production without significant cost increases. The economic and abundant nature of these materials makes them attractive for widespread commercial adoption in the battery industry [57].

2.3.4 Cycle Life

Cyclic life span of a battery is significantly influenced by the stability of its anode material. SnS, with improvements in material processing techniques, has shown enhanced cycle life despite its high capacity. ZnS typically exhibits better cycle life stability, thanks to its inherently stable and less reactive chemical nature. This makes ZnS particularly valuable in applications where battery reliability and longevity are critical [58].

2.3.5 *Tuneability and Safety*

Both SnS and ZnS offer tuneability in their physical and chemical properties through methods like doping or compositing with other materials, which can optimize their performance for specific applications. Furthermore, their good safety profiles makes them appropriate for use in consumer electronics and other implementations where safety is paramount. ZnS is noted for its inherent chemical stability, which enhances its safety characteristics, minimizing the risks associated with thermal runaway and electrolyte decomposition [59].

2.4 **Composite and Nanostructured in SnS Anode Material**

Tao et al., (2014), used one step hydrothermal synthesis process in the synthesis of SnS/graphene nanocomposites. Reagents employed were thiourea, stannous chloride dihydrate, and graphite oxide. Different characterization methods like X-ray diffraction, Field emission-scanning electron microscopy, Transmission electron microscopy, High resolution-transmission electron microscopy and Raman examination were employed. The morphology of synthesized material was further evidenced through uniformly dispersed SnS nanoparticles on graphene sheets. Electrochemical performance of anode material revealed that at 50 mAg^{-1} current density the composite delivered 535 mAg^{-1} over 50 cycles and 89 % coulomb efficiency in the second cycle. From EIS analysis, there was a smaller charge transfer resistance in the composite than that for pristine SnS alone [60].

Qayyum et al., (2020), employed solvothermal process to prepare SnS/CNTs and nitrogen, sulfur, cobalt-doped SnS/CNTs composite anode-material for Na-ion batteries. The reagents were used as $\text{SnCl}_2 \cdot 2\text{H}_2\text{O}$, thiourea, and carbon nanotube. The following characterization techniques that were used include XRD, SEM with EDS and EIS. Structure of nanocomposites was also established with fields of cauliflower-like structures linked by CNTs. The electrochemical-performances were characterized by using cyclic-voltammetry (CV), GCD galvanostatic charge-discharge tests. At current-density of 0.1 Ag^{-1} , the capacity of discharging of the nanocomposite was still as high as 183.71 mAhg^{-1} after fifty cycles. Electrochemical impedance spectroscopy measurements showed that the resistance of charge transfer of the nanocomposite was lesser than the bare electrode,

which pointed towards the enhanced application of the nanocomposite electrode as an anode for Na-ion batteries [61].

Tang et al., (2020), used a hydrothermal method combined with annealing to prepare Ti_3C_2 MXene@C@SnS composites which had the structure resembling a layered rock formation. The pertinent chemicals of the study were Ti_3C_2 MXene, $\text{SnCl}_4 \cdot 4\text{H}_2\text{O}$, TAA (thioacetamide) and glucose. The characterizations include mainly structural and morphological analysis by SEM, HR-TEM, XRD analysis, surface-specific Raman spectroscopy, XPS, and BET analysis of nitrogen adsorption-desorption isotherms. The nanocomposite also had a high specific surface-area with round about $255.78 \text{ m}^2/\text{g}$ or more and a high level of porosity, the existence of which is also apparent based on the results of the work on morphology. Electrochemical tests demonstrated impressive working, with a reversible-capacity of 1473 mAhg^{-1} at a current density of 0.1 Ag^{-1} . It maintained 1050 mAhg^{-1} over 350th cycle at 1 Ag^{-1} , with excellent rate performance, long-cycle stability. EIS analysis showed that material has lower charge-transfer resistance in comparison with controls which specify that the facilitated diffusion of lithium-ion and electron transfer characteristics exist in this composite [62].

Xiong et al., (2020) utilized an electrostatic self-assembly method to prepare SnS NPs anchored on 3D NG for improving the electrochemical performance. The chemicals employed were tin-chloride pentahydrate, thioacetamide, and graphene oxide, PDDA was used as a functionalizing reagent. The following characterizations were used such as SEM, HRTEM, XRD, Raman and XPS analysis. The electro-chemical activity was examined using cyclic voltammetry, GCD and EIS. The SnS/3D NG composite exhibits high cycle stability in sodium-ion batteries that have a great reversible-capacity of 509 mAhg^{-1} for 1000 cycles at 2 Ag^{-1} current density. This structural characteristic helped in the low charge transfer resistance with high electrical conductivity which in turn boosted the cycles as well as the rate capability of the 3DNG composites anodic material.

Dang et al., (2021), utilized an in-situ vulcanization synthesis technique for preparation of honeycomb like SnS/C composites material. The reagents used in this work are silica spheres, allyl thiourea, and tin (II) chloride dihydrate. Characterization by SEM,

HRTEM, XRD, Raman spectroscopy, XPS, BET, TGA was conducted for analysis as well. The construction, morphology of SnS/C was explained to be honeycomb like and the electrochemical performances were tested using CV and GCD tests. At 0.1 Ag^{-1} , the composite possessed a specific-capacitance of 607 mAhg^{-1} and possessed high-rate capability (313.2 mAhg^{-1} at 3 A g^{-1}) and cycling stability (404.7 mAhg^{-1} after 300 cycles at 1 Ag^{-1}). From the EIS measurements the values of charge transfer resistance were substantially lower than for undoped samples proving better lithium ion and electron transfer [63].

Cheng et al., (2022), engaged a plasma milling method to prepare tin sulfide–molybdenum disulfide–graphene (SnS-Mo-GNs) nanosheets. The following characterizations were used to examine the synthesized material such as X-ray diffraction, scanning electron microscopy, high-resolution transmission electron microscopy, XPS and Raman spectroscopy were done. Morphology revealed SnS embedded with Mo and graphene with the formation of micro/nano structure was evident. Electrochemical studies showed that at 0.1 Ag^{-1} , the composite has a higher discharge capacity of 1128 mAhg^{-1} over 600 cycles it exhibited initial Coulombic efficiency was found to be 86%. 9%. This was further evidenced from the Nyquist plots from EIS where the charge-transfer resistance of the material formed was lower [64].

Cheng et al., (2022), utilized a facile hydrothermal process followed by calcination to synthesize SnS/N-doped carbon reduced graphene oxide (SnS@N-C/rGO) composites. The reagents materials used in the experiment were $\text{SnCl}_4 \cdot 5\text{H}_2\text{O}$, thioacetamide, graphene oxide dopamine hydrochloride. The subsequent characterizations were used to find the synthesized material such as (XRD), (SEM), (HRTEM), (XPS) and Raman spectroscopy were done. Electrochemical performance revealed promising features with capacitance of 885 mAhg^{-1} . at 1.0 Ag^{-1} after 550th cycle [65].

Wang et al., (2024), used a facile solvothermal synthesis process for the growth of Ce-doped SnS micron-flowers on nickel foam as Ce@SnS/NF. The chemicals reagents were used as cerium nitrate, tin chloride, thiourea and cetyltrimethylammonium bromide (CTAB) in ethylene glycol solution. The subsequent characterizations were used to study

the synthesized material such as X-ray diffraction, scanning electron microscopy, high-resolution transmission electron microscopy, X-ray photoelectron spectroscopy and Raman spectroscopy were done. The electrochemical performance as cyclic voltammetry analysis revealed the specific-capacitance of 2549 F/g for Ce@SnS/NF at current-density of 2 Ag^{-1} , Its capacity decreases to 5% of this capacity after 10,000th cycle at 10 A/g currents density [66].

Xiao et al., (2024), successfully developed a 3D hierarchical porous carbon (HPC) structure enshrouded with flake SnS to increase the electro-chemical resources of LIBs. The raw materials used were tin chloride, thiourea, PAN and PVP. Techniques used to characterize the synthesized material include X-ray diffraction scanning electron microscopy, transmission electron microscopy, X-ray photoelectron spectroscopy, and nitrogen adsorption-desorption isotherms. There was a well-developed 3D HPC structure in the nanocomposites that improved charge transfer, minimized particle volume swelling, and presented more storage places for ions. Cycling Stability also showed that the SnS/HPC as anode offered a discharge-capacity of 917 mAhg^{-1} at 0.1 Ag^{-1} current density over 100 cycles [67].

2.5 Composite and Nanostructured in ZnS Anode Material

Peng et al., (2020), used a facile hydrothermal process followed with heat treatment process to prepare ZnS/rGO/S nanocomposites anode material. The reagents were used as zinc chloride, thiourea, and GO as raw materials.

The following techniques were used to investigate the synthesized material such as (XRD), (SEM), (HRTEM), (XPS) and Raman spectroscopy were done SEM and TEM characterization techniques were used as well. Electrochemical measurements indicated that at 0.2C, the ZnS/rGO/S composite has specific capacitance value of 645 mAhg^{-1} for 200th cycle [68].

Pathak et al., (2021), used an acid assisted ultrasonication process followed heat treatment for synthesis of ZnS/g-C₃N₄ composites material. The reagents used were zinc acetate, thioacetamide and g-C₃N₄ (graphitic carbon nitride). The subsequent

characterization techniques were used to investigate the synthesized material such as (XRD), (SEM), (HRTEM), (XPS) and Raman spectroscopy were done.

The electrochemical performance like GCD ZnS/g-C₃N₄ composite anode material exhibits specific capacity 596 mAhg⁻¹ at 1150th cycle at current-density of 1 Ag⁻¹. Decreased values were obtained in EIS measurements for charge transfer resistance which suggested better electrochemical performance [44].

Cao et al., (2021), utilized a novel approach ZnCo-ZIF for the synthesis of ZnS/CoS heterostructures that are well incorporated into the 3D N-doped CNTs network (ZnS/CoS-NCNTs). The reagents used for synthesis were Zinc Nitrate, Cobalt Nitrate and 2-methylimidazole. The additional characterization techniques (XRD), (FESEM), (HRTEM) and (XPS).

The uniform distribution of nano-sized ZnS/CoS heterostructure in N-doped CNTs was again affirmed with this morphology which can be described as ZnS/CoS-NCNTs. Electrochemical analysis showed better performance with a reversible capacity of 1007 mAhg⁻¹ on the initial rate of 1.0 Ag⁻¹ after 1000 cycles, and 803 mAhg⁻¹ at 5. It displays an brilliant rate capability and cyclic stability and keeps 94.93% of its initial capacity at 5.0 Ag⁻¹ after 2000 cycles [69].

Luo et al., (2023), achieved ZnS@MoS₂ nanoparticles embedded in N-doped carbon with rGO (ZnS@MoS₂/NC@rGO) using a sulphuration reaction. The reagents used were Zn(NO₃)₂·6H₂O, (NH₄)₆Mo₇O₂₄·4H₂O, 2-methylimidazole and graphene oxide. Advanced characterization methods such as XRD, SSEM, TEM, and XPS were used.

Morphology of the nanocomposite was also verified by having a hierarchical nanostructure. Electrochemical measurement indicated that at 0.2 Ag⁻¹ current density, the ZnS/MoS₂ composite was able to deliver 480 mAhg⁻¹ capacity for 100 cycles [70].

Wang et al., (2024), used a facile hydro-thermal process to synthesize hetero structures of ZnS-Co embedded in nitrogen-doped graphene. The following materials used during the synthesis process were zinc Chloride, cobalt acetate, as well as graphene oxide.

The corresponding characterization were used to study the synthesized material such as X-ray diffraction, scanning electron microscopy, high-resolution transmission electron microscopy, X-ray photoelectron spectroscopy and Raman spectroscopy were done. The ZnS-Co heterostructures exhibits specific capacity of 1210 mAhg^{-1} at 1 Ag^{-1} current-density and with stable cyclability over 500 cycles [71].

Hu et al., (2024), synthesized ZnS/C–SnO₂–BaSO₄ composite materials by a facile hydrothermal technique followed with ball milling. Following characterization tools were use as Electron microscopy techniques like SEM, HRTEM and XPS based characterization techniques were also carried out.

The composite exhibited enhanced electrochemical character in sodium-ion batteries with specific capacities 301 mAhg^{-1} at 50 mAg^{-1} at 50th cycle [72].

Zhang et al., (2022), prepared ZnS-ZnSe heterostructure by using chemical vapor deposition method. Materials which were used comprised of zinc acetylacetonate and selenium powder. XRD characterization also showed the presence of heterostructure while SEM and TEM provide evidence of a hierarchy structure that greatly favors electrochemical properties.

In the ZnS-ZnSe heterostructures a remarkable electrochemical performance was observed; they reserved a stable capacitance value of 850 mAhg^{-1} in the discharge at 0.5 Ag^{-1} over 400 Cycles. The enhancement of the performance was due to the synergistic action between ZnS and ZnSe, which helped in the synthesis of a good ion conducting network for transporting ions and electrons [65].

2.6 Binary Metal Sulfide Based Composites

Binary metal sulfide SnS:ZnS gaining attentions due to their higher specific capacity and synergistical effect which induce the build in electric field between the heterostructure which boost the electrochemical performances of energy devices so few heterostructures anode materials are reported on Li as well as for Na-ion batteries are given bellow:

Table 2.1: Literature survey of SnS:ZnS based composites.

Active Material	Year	Author / Journal	Main Findings	Ref.
SnS:ZnS particles coated with nitrogen doped carbon sheets	2024	Ping Xu et al./Materials Letters	The Solvothermal synthesis method used, at a 0.1 current density the initial discharge was 1135.5 mAhg ⁻¹ and exhibited a specific capacity value of 880 mAhg ⁻¹ at 0.1 A/g after 100 cycles with 98% retentions.	[66]
ZnS:SnS-Sb ₂ S ₃ @C	2023	“Miao-Ling Chen et al. / ChemNanoMat”	The Cation-exchange synthesis method used, exhibited a reversible specific capacity of 581 mAhg ⁻¹ at 1 A/g after 100 th cycle	[73]
Heterostructure ZnS:SnS@N-doped C	2022	“Lixuan Zhang et al. / Journal of Alloys and Compounds”	Hydrothermal method gives yolk shell microspheres, exhibited a reversible specific capacity of 775.5 mAhg ⁻¹ at 200 mA/g after 100 cycles and maintains capacity 571.2 mAhg ⁻¹ after 1000 cycles at 1 A g ⁻¹ .	[74]
ZnS:SnS heterostructure	2022	“Dongyu Bian et al. / Journal of Alloys and Compounds”	The vulcanization or carbonization method used to give hollow SnS/ZnS nano box, exhibited a reversible specific capacity of 553.5 mAhg ⁻¹ after 100 cycles, at 0.2 and 62.3% retentions obtained at 5A/g.	[75]

ZnS:SnS@NC heterostructure	2021	“Weiqi Yao et al. / ACS Nano”	The vulcanization or carbonization method used to give hierarchical SnS/ZnS showed a specific capacity of 1149 mAhg ⁻¹ at 0.2 A/g for 300cycles and 661 mAhg ⁻¹ at 10.	[76]
ZnS-SnS@NC heterostructure with Graphite	2021	“Qinqin Liang et al. / Chemical Physics Letters”	The coprecipitations method used to embed the nanoparticles on GO sheets, exhibited a specific capacity of 517 mAhg ⁻¹ at 1 A/g over 600 cycles.	[77]
ZnS:SnS@CNTs ZnS:SnS@GO	2021	“Afifa Sadaqat et al. / ACS Applied Energy Materials”	The Solvothermal method used to synthesized SnS:ZnS hetrostructure, exhibited a specific capacity of 343 and 364 mAhg ⁻¹ at 0.1 A/g over 100 cycles for graphene oxide and carbon nanotubes respectively.	[78]
ZnS:SnS heterostructure	2022	“D. Bian et al. / Journal of alloy and compound”	The Solvothermal method used to synthesized SnS:ZnS heterostructure, exhibited a specific capacity of 672 mAhg ⁻¹ at 1 A/g current density over 500 cycles	[75]
ZnS:SnS@C heterostructure	2019	“Jinjin Ai et al. / Applied Surface Science”	The Hydrothermal method used to synthesize SnS/ZnS@C heterostructure, exhibited a initial specific capacity of 921 mAhg ⁻¹ at	[79]

			200 mA/g and reversible capacity 485 mAhg ⁻¹ over 250 cycles.	
“ZnS:SnS@C heterostructure	2019	“Yu Zhang et al. / Chemical Engineering Journal”	The vulcanization or carbonization method used to synthesize nano box SnS/ZnS exhibited an initial specific capacity of 912 mAhg ⁻¹ at 0.1 A/g and maintained 492 mAhg ⁻¹ over 300 cycles.	[80]

CHAPTER 3: MATERIALS AND METHODS

This chapter contribute a complete description of the synthesis protocols of materials, including Graphitic Carbon Nitride, ZnS, SnS, SnS:ZnS composite and ternary composite SnS-ZnS@g-C₃N₄. These materials are synthesized as an anode material in lithium-ion batteries, and each section details the respective procedures.

3.1 Reagents and Chemicals

The following reagents and chemicals were employed in the synthesis processes:

- Zinc Chloride (ZnCl₂)
- Tin Chloride Dihydrate (SnCl₂·2H₂O)
- Sodium Sulfide Nonahydrate (Na₂S·9H₂O)
- Ethylene Glycol (EG)
- Urea
- Ethanol
- Deionized Water (DI)

3.2 Synthesis of Material

3.2.1 *Synthesis of ZnS*

The formation of ZnS nanoparticles was done using zinc chloride (ZnCl₂) and sodium sulfide nonahydrate (Na₂S·9H₂O) as precursors. First, 15 mmol of ZnCl₂ was dissolved in 15 mL of distilled water and 5 mL of ethylene glycol under constant stirring till homogeneous clear solution was obtained. At the same time, a sodium sulfide solution was prepared by diluting 50 mmol of Na₂S·9H₂O in 50 mL of distilled water. The sodium sulfide solution was subsequently allowed to be added dropwise in the zinc chloride solution with the help of stirring. The obtained mixture was stirred for 30 minutes to favor

the formation of zinc sulfide nanoparticles as well as to improve their dispersion by sonication for 1 hour.

The obtained mixture was then sonicated and after sonication the reaction mixture was transferred into a Teflon lined autoclave and heated at 200 °C for 10 hours for hydrothermal synthesis of ZnS nanoparticles. After the hydrothermal process, the autoclave was cooled to room temperature without intervention. The obtained ZnS nanoparticles were then pelleted and washed with ethanol and de-ionized water several times to get rid of any remaining impurities and then placed in vacuum oven for drying for 24 hours at 60°C to yield the refined ZnS powder.

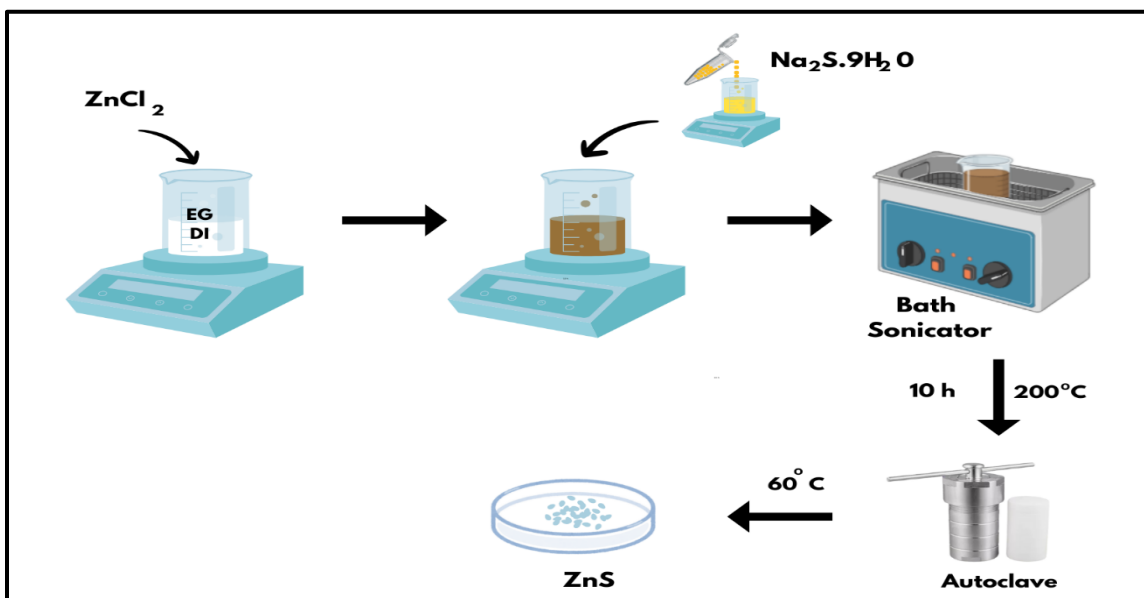


Figure 3.1: Schematic Illustration of ZnS Synthesis.

3.2.2 Synthesis of SnS

In the formation of the tin sulfide (SnS) nanoparticles, tin(II) chloride dihydrate (SnCl₂·2H₂O) and sodium sulfide nonahydrate (Na₂S·9H₂O) were employed as the major precursors. SnS was synthesized by dissolving 15 mmol of SnCl₂·2H₂O in 15 mL deionized water and 5 mL EG under constant stirring until a clear solution was obtained. At the same time, sodium sulfide solution was prepared in which 50 mmol of Na₂S·9H₂O was dissolved in 50 mL of deionized water. It was then combined with the tin chloride solution accompanied with continuous stirring to enhance the mixing of sodium sulfide

solution. Then solution mixture was sonicated to increase the homogeneity and dispersion in the resulting mixture.

After sonication, the mixture was placed in a Teflon-lined autoclave and placed in oven at 200 °C for 10 hours. This enhanced the hydrothermal process that helped in the creation of SnS nanoparticles. Following the heating period the autoclave was allowed to cool at room temperature without any intervention. The SnS were then separated from the solution by centrifugation with multiple ethanol and deionized water cycle to ensure the removal of any unwanted residues, and the final SnS powder obtained by drying the product at 60 °C for 24 hours.

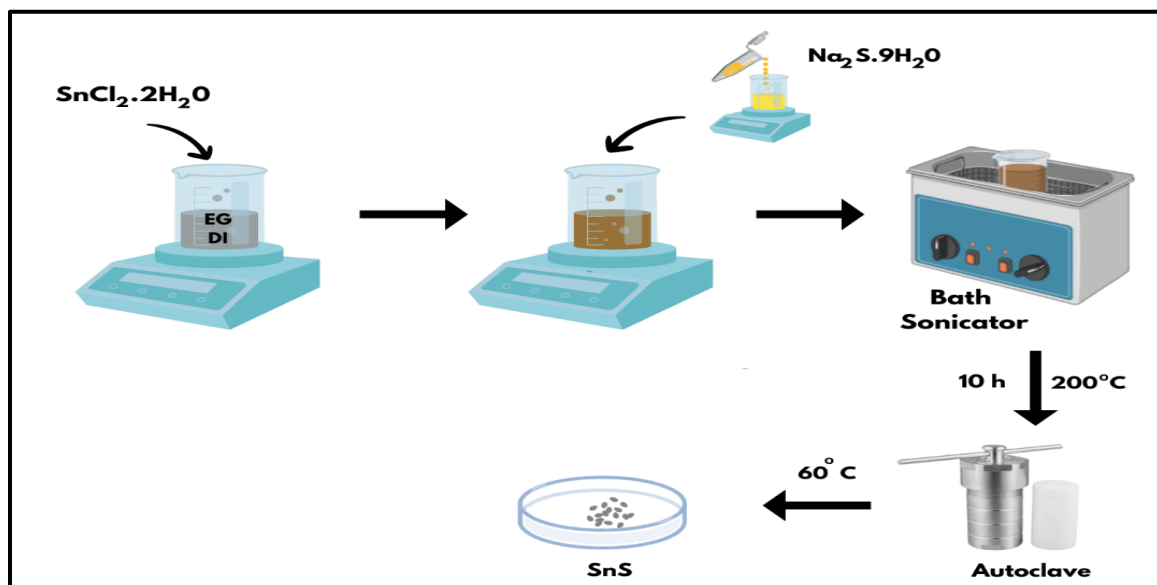


Figure 3.2: Schematic Illustration of SnS Synthesis

3.2.3 Synthesis of SnS:ZnS Composite

Synthesis of SnS:ZnS composite started with the preparation of zinc and tin chloride solutions. For preparing the zinc chloride solution, 15 mmol of ZnCl_2 was dissolved in 15 mL of de-ionized water to which 5 mL of ethylene glycol has been added to ensure homogeneity. In the same way, 15 mmol of $\text{SnCl}_2 \cdot 2\text{H}_2\text{O}$ was dissolved in the 15 ml of DI water and 5 ml of ethylene glycol to make tin chloride solution.

When both solutions are prepared the tin chloride mixture was slowly added drop wise to the zinc chloride solution drop by drop while stirring simultaneously. This addition resulted in a milky appearance of the mixture and the solution was stirred vigorously for another 10 minutes. To allow additional reaction to occur, 50 mmol of the sodium sulfide was prepared by dissolving $\text{Na}_2\text{S}\cdot 9\text{H}_2\text{O}$ in 50 mL of distilled water. This solution was then added to the milky Zn-Sn mixture and vigorously stirred. This mixture solution was then placed in an ultra-sonication bath for 1 hour to get homogenous dispersion.

After sonication the brownish liquid was shifted to Teflon-coated autoclave and the reaction mixture was heated at 200°C for 10 hours. This hydrothermal treatment promotes the crystallization and growth of the SnS:ZnS composite under high temperature and pressure. The autoclave was left to cool to room temperature, a process that enhances the achievement of distinct nanoparticles.

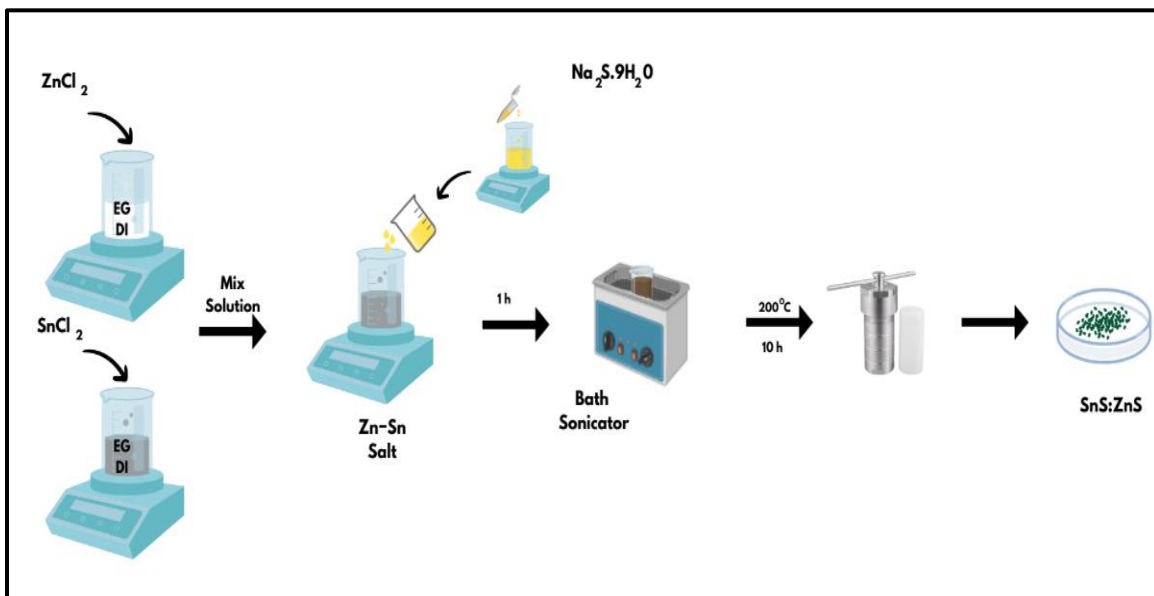


Figure 3.3: Schematic Illustration of Synthesis of SnS-ZnS

After cooling, centrifugation was performed by rinsing the solution many times with ethanol and deionized water to remove any remaining reactant or any impurities. Lastly, the purified composite was dried in an oven at 60°C overnight. This drying process ensures the removal of any remaining moisture, resulting in a fine, dry powder of the SnS:ZnS composite.

3.2.4 Synthesis of Graphitic Carbon Nitride

The Graphitic Carbon Nitride ($g\text{-C}_3\text{N}_4$) was prepared using a straightforward thermal treatment process. 15 grams of urea were taken and placed into a 50 ml ceramic crucible. The crucible was then covered with the lid and was then securely wrapped with aluminum foil.

It was then placed in a muffle furnace that had been pre-heated at 550 degrees Celsius. Finally, the temperature was raised gently from room temperature at a rate of 10°C per minute till the required temperature was achieved. The furnace was then set at 550°C and held there for 4 hours. This was then followed by allowing the furnace down to room temperature for a couple of hours. Following the cooling process, the crucible was carefully taken out of the furnace. The enhanced yield was achieved through a high-temperature treatment of the precursor to obtain the $g\text{-C}_3\text{N}_4$ and the yield was in the form of a yellow powder.

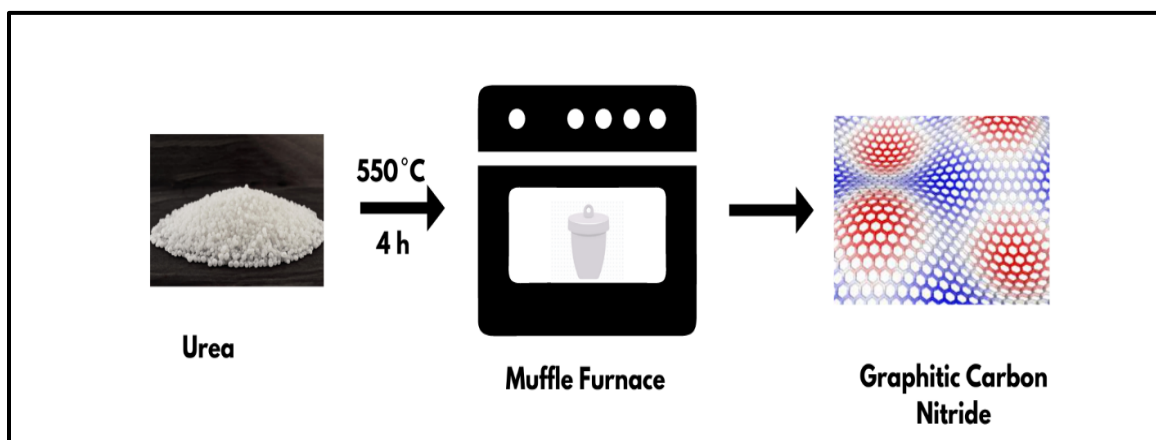


Figure 3.4: Schematic Illustration Synthesis of $g\text{-C}_3\text{N}_4$.

3.2.5 Synthesis of $\text{SnS}:\text{ZnS}@g\text{-C}_3\text{N}_4$

The synthesis of the $\text{SnS}:\text{ZnS}@g\text{-C}_3\text{N}_4$ was done by incorporating graphitic carbon nitride ($g\text{-C}_3\text{N}_4$) into the $\text{SnS}:\text{ZnS}$ matrix. Initially, $\text{SnS}:\text{ZnS}$ composite was synthesized by the process explained above. When it's done, 200 mg of graphitic carbon nitride ($g\text{-C}_3\text{N}_4$) sheets are also introduced to the above mixture during sonication so that the $g\text{-C}_3\text{N}_4$ is

uniformly dispersed in the SnS:ZnS composite. The sonication facilities, the blending of the g-C₃N₄ and the materials combine well making them homogenous.

After sonication the mixture was transferred to Teflon-coated autoclave and was heated at 200 °C for 10 hours. This hydrothermal treatment promotes the crystallization and growth of the g-C₃N₄ over SnS:ZnS composite. The autoclave was settled to cool to room temperature. After cooling, centrifugation was performed by rinsing the solution many times with ethanol and deionized water to remove any remaining reactant or any impurities. Lastly, the product was dried in an oven at 60°C for 24 hours.

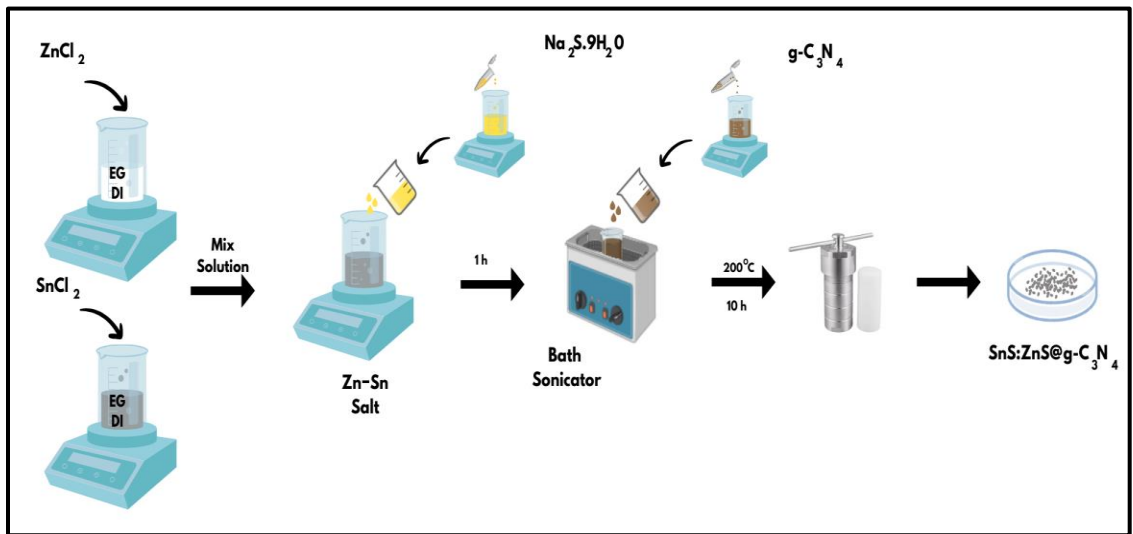


Figure 3.5: Schematic Illustration of SnS:ZnS@g-C₃N₄.

3.3 Fabrication of Electrodes

3.3.1 Slurry Preparation

- For slurry preparation, the weight ratio of active material was taken as 70:20:10, where carbon black was used as a conducting carbon, and PVDF (polyvinylidene fluoride) was used as a binder. The measurements were done carefully with the right calculations for making a proper slurry.
- These components were transferred into a clean glass reagent bottle and an appropriate amount of NMP (N-Methyl-2-pyrrolidone) is added to the mixture.

- The mixture was churned continuously for 24 hours to ensure a homogenous slurry was formed.



Figure 3.6: Slurry Preparation

3.3.2 Electrode Coating

- Initially, the surface of glass substrate and the notch bar was rinsed with acetone. The notch bar of thickness 200 μm was used. Acetone was sprayed on the glass substrate to attach the copper foil to the surface which serves as the current collector. After adhering to the Cu foil, it was further cleaned with the acetone.

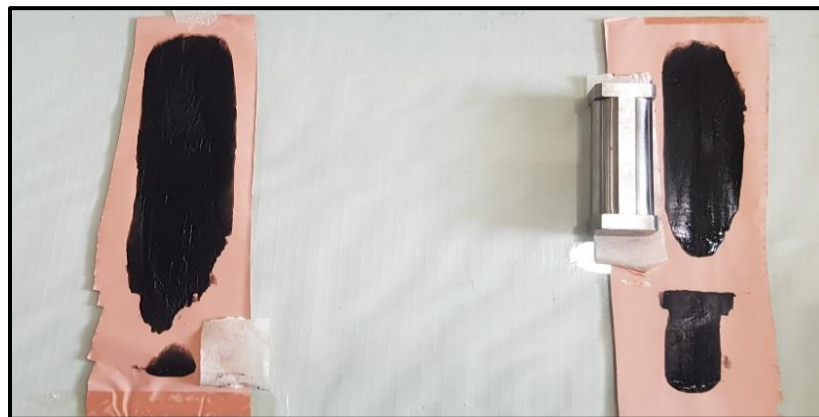


Figure 3.7: Representations of Pasted Slurry on a Cu Foil

- Slurry is pasted on the substrate using notch bar technique with different thickness. The slurry coated electrode was dried in the vacuum oven at 60 °C for 24 hours.

3.3.3 Electrode Calendaring



Figure 3.8: Representations of Calendaring Process

3.3.4 Electrode Punching

- After drying, material pasted Cu sheet was placed on the electrode disk cutter and circular electrodes with a diameter of 15mm were punched out.
- Try to avoid wasting the sheet and cut as many electrodes as possible. Remove the punched electrodes gently with the help of plastic tweezers and store them on respective butter paper. And finally, measure the weight of electrodes.

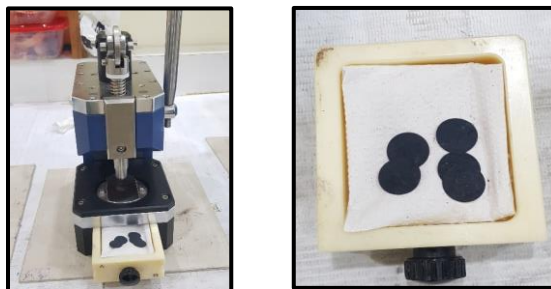


Figure 3.9: Representations of Electrode Cutting After Proper Drying

For optimal electrode performance, proper drying, precise measurements, clean working conditions, and careful handling are essential for achieving optimal electrode performance.

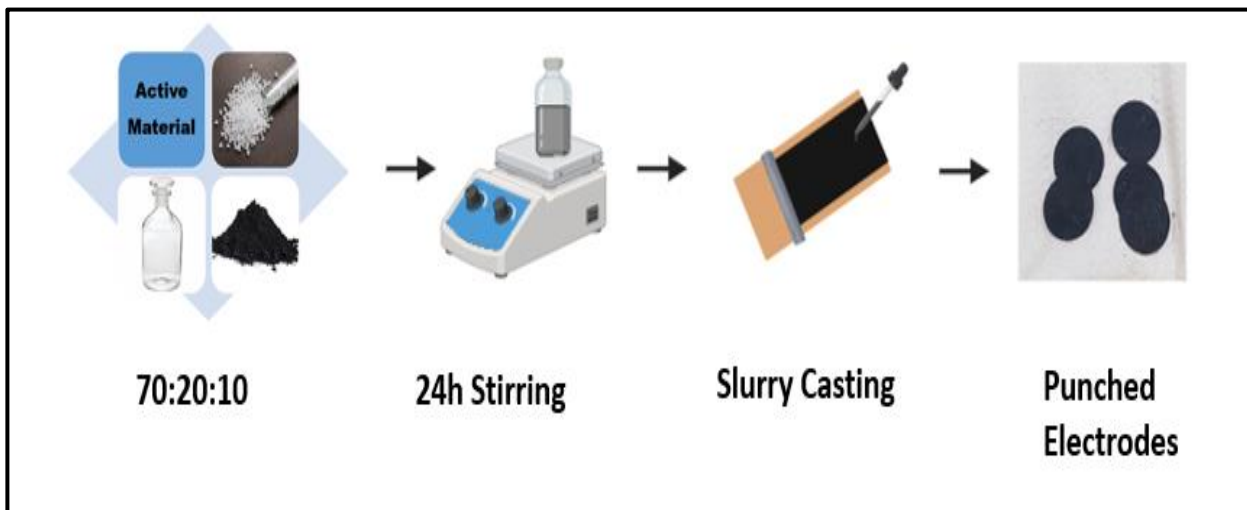


Figure 3.10: Flow Diagram of Electrodes Fabrication Process

3.4 Assembling of Cells

The coin cell assembly was carried out with careful attention to detail, ensuring that the cells would perform optimally. All assembly steps were completed in an argon-filled glovebox, where moisture and oxygen levels were strictly kept below 0.1 ppm to prevent contamination.

Extra care was taken to minimize any exposure of the glovebox's interior to the outside environment. To avoid damaging the glovebox gloves, sharp tools were not used inside. All tasks were performed slowly and carefully, taking about three times longer than they would outside the glovebox. Additional gloves were worn over the glovebox gloves while handling chemicals for added protection.

All components, including lint-free wipes, were heated in a vacuum oven at 60°C under a pressure of 0.1 MPa to remove any moisture before being brought into the glovebox.

The active material synthesized above served as the anode (negative electrode), while lithium metal foil was used as the cathode (positive electrode). A porous polypropylene (PP) separator was chosen, and the electrolyte solution was composed of 1M LiPF₆, mixed in a 2:1:2 ratio of ethylene carbonate (EC), dimethyl carbonate (DMC), and ethylene methyl carbonate (EMC)

- The assembly process began by placing the vials with all necessary components into the glovebox's antechamber.
- After sealing the hatch securely, the pressure was reduced to 0.1 MPa, and the chamber was filled with argon. This purging process was repeated 1-2 more times depending on the number of items.
- Initially, the coin cell parts were carefully laid out on clean tissue paper, following a specific sequence.



Figure 3.11: Coin cell fabrication process in a glove box.

- Using a micropipette, the prepared active material coated electrode was placed in the center of the lower casing of the coin cell, with the slurry-coated side facing upward.

- After adding 2-3 drops of electrolyte on the anode, plastic tweezers were used to carefully position the PP separator over it, followed by another 2-3 drops of electrolyte on the separator's center.
- Next, the lithium metal chip, serving as the cathode, was placed on top of the separator with its rough side facing up. The spacer was positioned with its edged surface facing up, followed by the conical spring, and these were then secured with the upper casing of the coin cell.

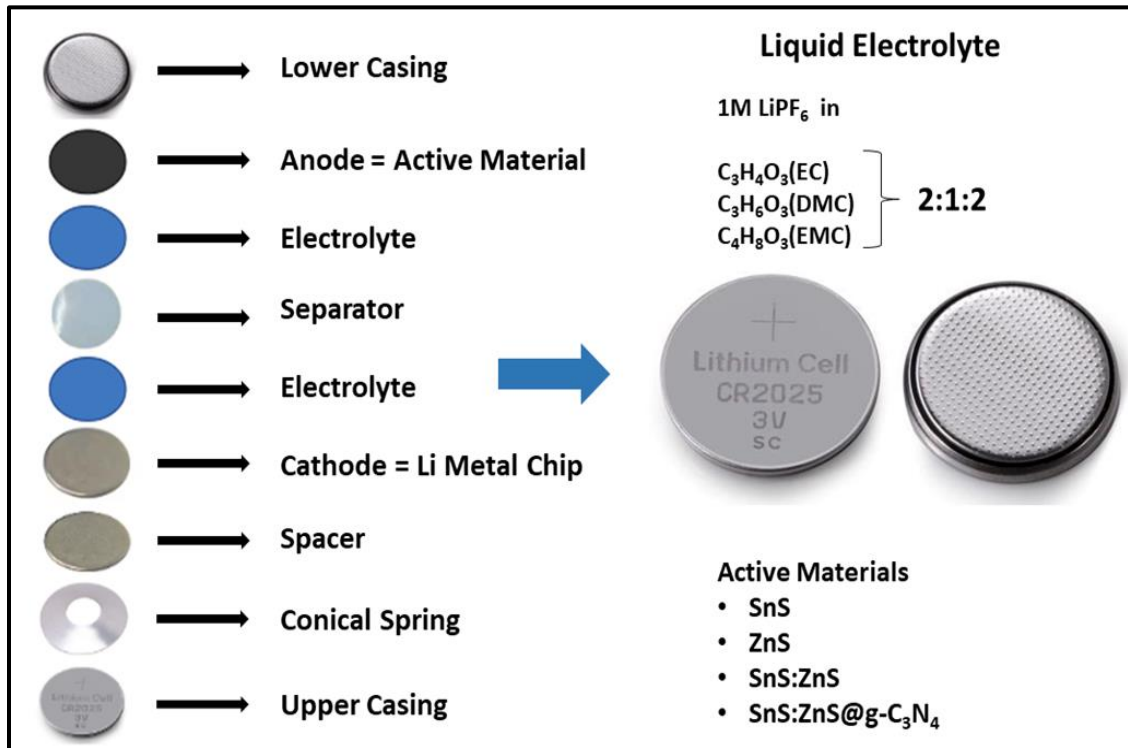


Figure 3.12: Steps for coin cell assembly.

- The assembled coin cell was then placed into the crimper, ensuring it was centered in the groove, and a crimping force of 6.2 MPa (900 psi) was applied before releasing it.
- After crimping, the cell was carefully removed, any excess electrolyte was cleaned off, and the process was repeated for additional cells.

- After cleanup, the assembled cells were labeled accordingly and removed from the glovebox.

The cells were then left to stabilize for 24 hours, and their voltage was measured. (If cell's voltage is below 2 V, it means cell has been short circuit and can no longer be used.) Once the cells had stabilized, they were ready for application-based testing and characterization.

CHAPTER 4: CHARACTERIZATION

4.1 Structural, Morphological and Compositional Analysis

4.1.1 X-Ray Diffraction Analysis (XRD)

The phase and crystal structure of prepared pristine graphitic nitride ($g\text{-C}_3\text{N}_4$ SnS, ZnS, SnS:ZnS, and ternary composites SnS-ZnS@ $g\text{-C}_3\text{N}_4$ was confirmed by XRD analysis, which are provided in **Figure 4.2**.

The typical XRD patterns for $g\text{-C}_3\text{N}_4$ shows two peaks at 13.1° and 27.51° corresponding in-plane trigonal nitrogen linkage of the tri-s-triazine units and the interlayer stacking of the conjugated aromatic systems, indexed as the (100) and (002) planes, respectively in **Figure 4.1** [81-84].

The diffraction patterns ZnS was well matched with JCPDS no: 01-077-2100 (17). The foremost diffraction peaks that appeared in ZnS XRD patterns at $2\theta = 28.47^\circ$, 32.82° , 47.53° , 56.38° correspond to (111), (200), (220), and (311) planes which reveals the structure of ZnS [85]. The XRD results of SnS exhibits the peaks at 21.97° , 25.98° , 27.43° , 30.44° , 31.49° , 31.63° , 31.93° , 39.01° , 42.42° , 44.76° , 45.46° , 48.49° , 51.26° , 53.10° , 54.20° , 64.14° with respective planes (110), (120), (021), (101), (111), (130), (040), (131), (210), (141), (002), (022), (151), (122), (061), and (251).

The strong XRD peaks of SnS were matched with the orthorhombic crystal system (JCPDS no: 01-075-1803) [86]. In the case of SnS-ZnS@ $g\text{-C}_3\text{N}_4$ composite, graphitic nitride peaks slightly shift towards higher angle due to incorporation of SnS:ZnS nanoparticles into it which results in decrease in interplanar distance, one more important thing is increase in intensity of ZnS in ternary composites due to dominance of ZnS nanoparticles which is confirmed by EDS data.

The final XRD pattern ensures the presence of SnS, ZnS and $g\text{-C}_3\text{N}_4$ phases. There is no more impurity peak in results, exposing the purity of synthesized materials.

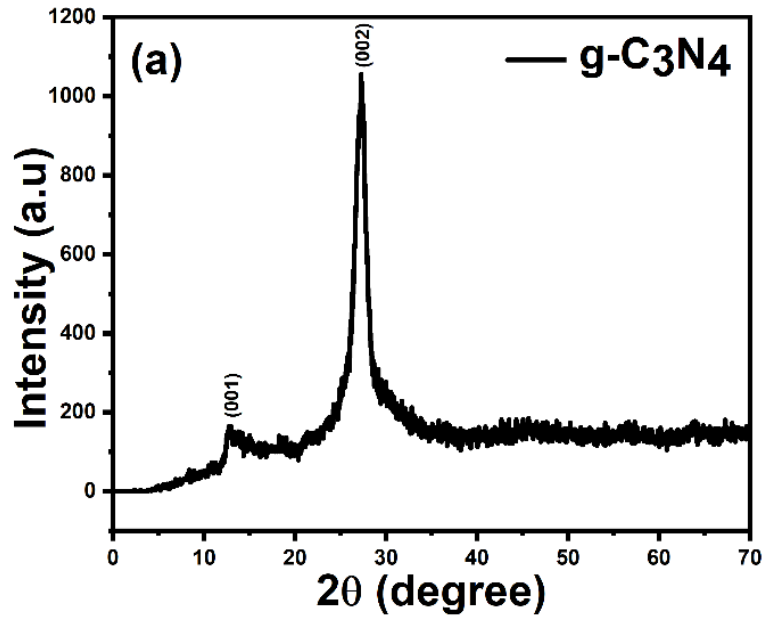


Figure 4.1: XRD spectra of g-C₃N₄ sheets

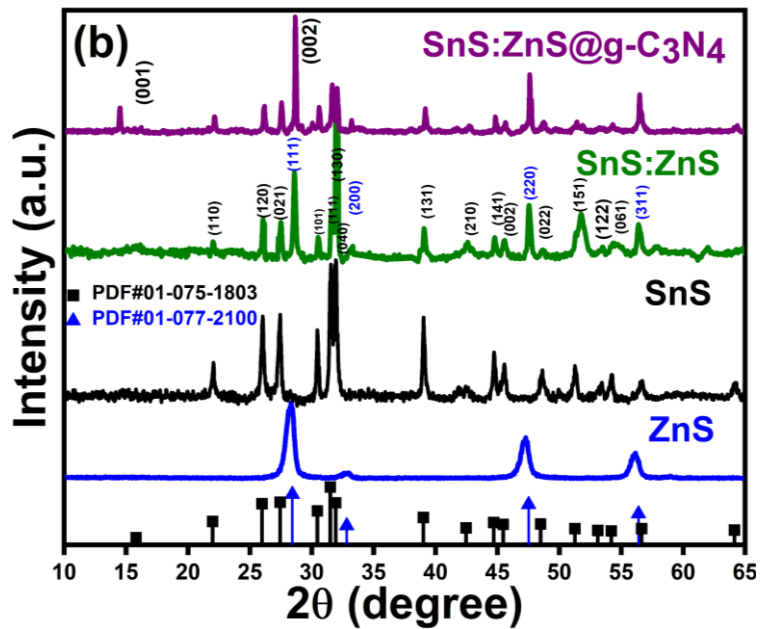


Figure 4.2: XRD Spectra of ZnS, SnS, SnS:ZnS and SnS:ZnS@g-C₃N₄

4.1.2 SEM Analysis

The detailed Morphology and microstructure analysis of SnS:ZnS, g-C₃N₄ and SnS:ZnS@g-C₃N₄ obtained were investigated using both scanning electron microscope

(SEM). **Figure 4.3 (a, b)** shows a 3D interconnected layered sheet like morphology of g-C₃N₄ composed of highly curved nanosheets with a wrinkled surface. The wrinkled sheet like structure provides the large surface area and porosity of the g-C₃N₄ [87]. Furthermore, **Figure 4.3 (c)** shows a uniform granular like nanostructured particles of SnS:ZnS [75].

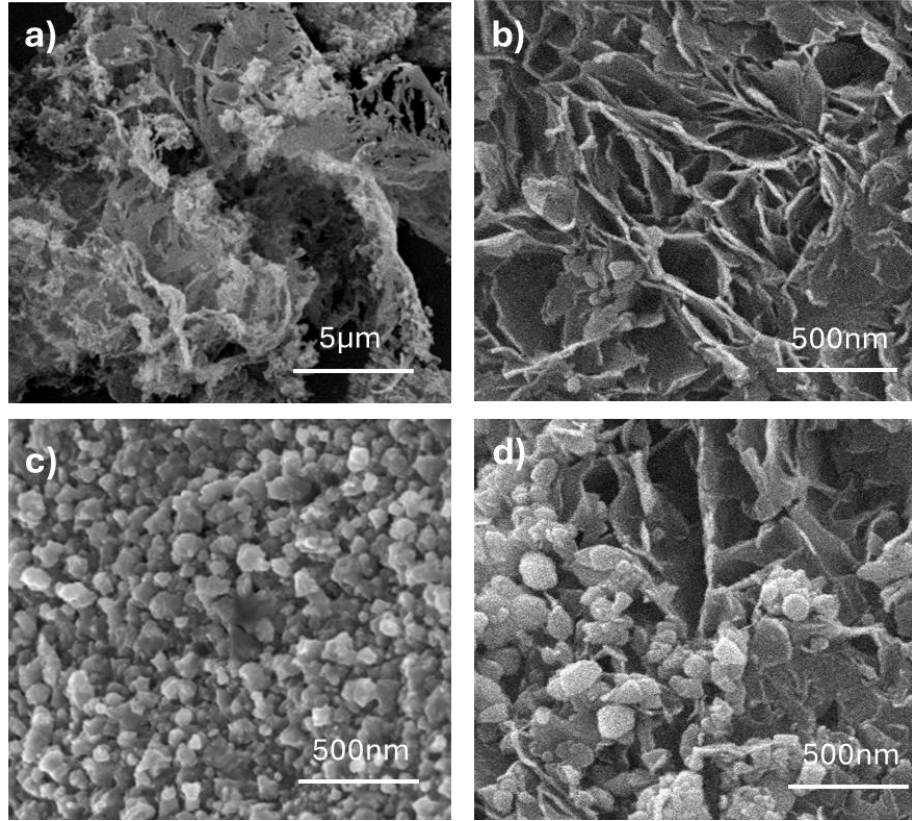


Figure 4.3: Lower and higher magnification SEM images of g-C₃N₄ 2D sheets (a, b) SnS:ZnS nanoparticles (c) Incorporation of SnS:ZnS on g-C₃N₄ 2D sheets (d)

These particles appear to be closely packed with a rough surface that provides abundant active sites for redox reactions. It is important to note that numerous SnS:ZnS heterostructures nanoparticles anchored onto the wrinkled surface of g-C₃N₄ sheets are observed in **Figure 4.3 (d)** and sheets can provide buffer space to accommodate the volume expansion of composites during lithiation and de-lithiation, decrease diffusion path of Li ions [88]. It is obvious that by the introduction of g-C₃N₄ with bimetallic SnS:ZnS nanoparticles synergistically increase the interfacial contacts and reduces the Li-ion diffusion path inside the active material.

To verify the elemental compositions of synthesized SnS:ZnS@g-C₃N₄ composite and g-C₃N₄, EDS analysis was conducted as shown in **Figure 4.4**. The presence of both carbon and nitrogen from g-C₃N₄ and ZnS:SnS components is clearly visible in the EDS spectra of the prepared nanocomposites [78].

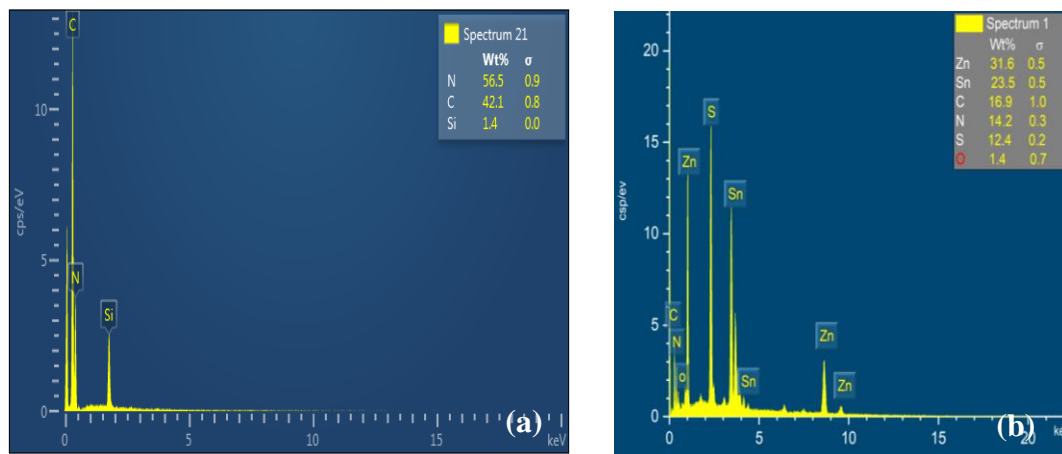


Figure 4.4: EDX spectra of g-C₃N₄ 2D sheets (a) and SnS:ZnS on g-C₃N₄

4.1.3 FTIR Analysis

The chemical structure and availability of various functional groups were analyzed using FT-IR spectra illustrated **Figure 4.5**.

The broad peak appearing in fingerprint region around 540 cm⁻¹ and at 619 cm⁻¹ corresponds to Sn-S and Zn-S stretching vibrations modes respectively, which confirming the formation of SnS and ZnS, C-O and C=O (arises due to ethanol washing) is also attached with pristine ZnS and SnS:ZnS composites which was removed in SnS:ZnS@g-C₃N₄ by proper washing.

The pristine g-C₃N₄ displays broad absorption bands between 3245 and 2900 cm⁻¹, corresponding to the stretching vibrations of N-H and O-H bonds, while a sharp peak at 809 cm⁻¹ can be attributed to the s-triazine rings breathing vibration out-of-plane.

Additional peaks at 1251 cm⁻¹, 1320 cm⁻¹, 1403 cm⁻¹, and 1540 cm⁻¹, 1650 cm⁻¹ are assigned to the stretching vibrations of the C-N heterocyclic ring. A prominent peak at 1637 cm⁻¹ is associated with the C=N stretching vibration [89, 90].

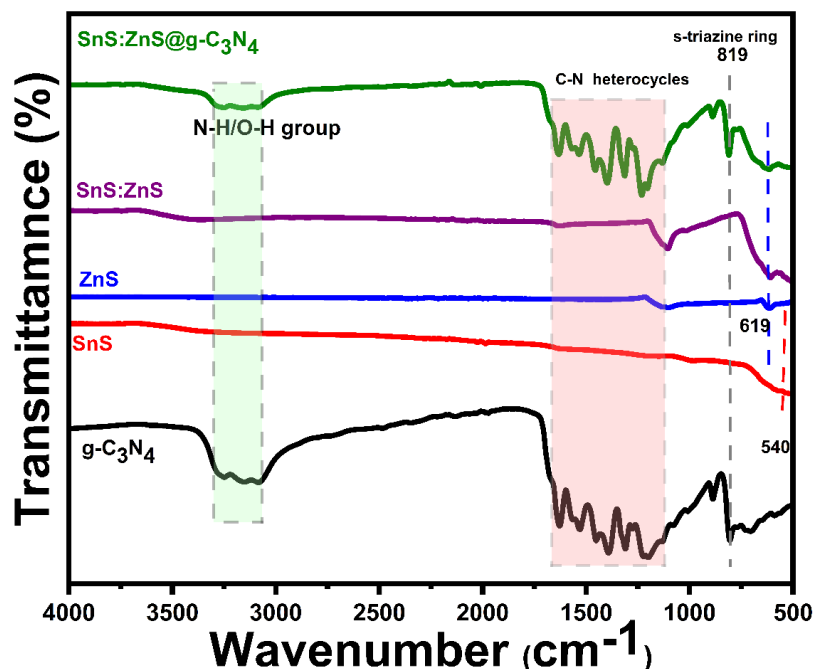


Figure 4.5: FTIR spectra of g-C₃N₄, SnS, ZnS, SnS:ZnS and SnS:ZnS@g-C₃N₄ composite

4.1.4 XPS Analysis

The XPS investigation was carried out to reveal the chemical composition and oxidation states of elements in SnS:ZnS@g-C₃N₄ composites. **Figure 4.6** shows the survey spectrum, which consists of Sn, Zn, C, N and S confirming the presence of respective elements in the ternary composite. Surface chemistry and composition of the SnS:ZnS@g-C₃N₄ ternary composite, which demonstrates significant promise as an anode material for lithium-ion batteries (LIBs). The **Zn 2p** peaks at 1021.6 eV and 1044.6 eV confirm the presence of Zn²⁺ in ZnS, illustrating successful integration of ZnS within the composite structure [74]. The **Sn 3d** peaks at 486.1 eV and 494.5 eV correspond to Sn²⁺ in SnS, with additional peaks at 487.6 eV and 496.2 eV indicating the presence of Sn⁴⁺, suggesting partial oxidation to SnO₂ [59]. These mixed valence states contribute to the enhanced electrochemical activity during cycling. The **S 2p** spectrum, with peaks at 161.8 eV and 163.0 eV, indicates the presence of S²⁻, confirming the formation of metal sulfides, while a peak at 168.9 eV represents SO₄²⁻, suggesting some surface oxidation. The **C 1s** spectrum shows peaks for graphitic carbon (C-C/C=C) and C-N/C-S bonds, highlighting strong

interactions between the carbon matrix and the active materials, providing enhanced conductivity and structural stability. Furthermore, the N 1s spectrum shows peaks for pyridinic-N, pyrrolic-N, and graphitic-N, which are known to improve electron transport and electrochemical performance in LIBs [91]. This combination of ZnS, SnS, and g-C₃N₄, along with mixed oxidation states and robust carbon-nitrogen bonding, enhances lithium-ion storage properties by mitigating volume expansion, ensuring fast ion/electron transport, and providing structural stability, akin to similar studies focused on advanced lithium-ion anode materials.

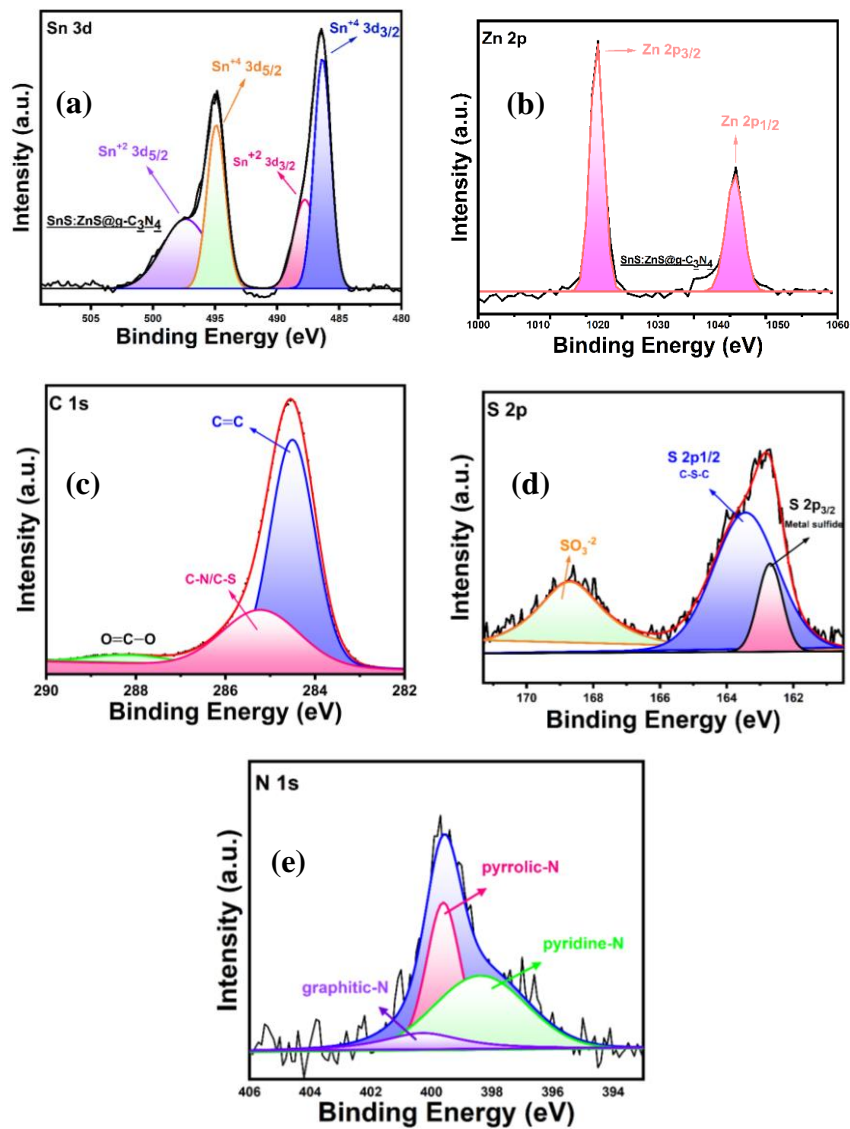
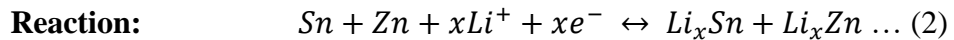
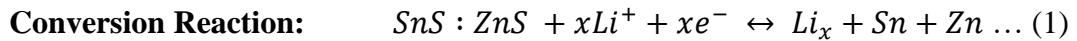


Figure 4.6: Higher Resolution XPS spectra (a) Sn 3d (b) Zn 2p (c) C 1s (d) S 2p (e) N 1s

4.2 Electrochemical Measurements

4.2.1 Cyclic Voltammetry

To investigate the electrochemical properties of synthesized SnS:ZnS@g-C₃N₄ composites cyclic voltammetry measurements were performed at scan rate 0.5 mVs⁻¹ in the voltage range of 0.01-3.0V vs Li/Li⁺ electrode. **Figure 4.7** reveals important insights into the electrochemical behavior of the composite material as an anode. In the first cathodic scan one sharp located at 0.88 V and a small peak at 0.69V are typically associated with the formation of the solid electrolyte interphase (SEI) layer and certain irreversible reactions. The peak situated at 0.52V and a shoulder at 0.13V assigned to conversion reactions of SnS and ZnS to their respective metal states (Sn and Zn), along with Li₂S formation. The decreases in peak intensity in the subsequent cycles are owed to the gradual stabilization of the SEI layer. In the subsequent anodic scan, the sharp peak centered at 0.72V and an adjacent shoulder at 0.64V are attributed to the oxidation of Li₂Sn to SnS and graphitic carbon nitride respectively. The peak located at 1.41V and the peak at 1.90V are assigned to the conversion of Li₂Zn to ZnS and Li₂S to Li-metal respectively with a broad peak at 2.44V assigned to the decomposition of SEI layer. The overall anodic process involves the oxidation of metal alloys suggesting extraction of lithium ion from the metallic Sn and Zn phases as well as the reformation of metal sulfides [92]. In the following cathodic as well as anodic cycle the peak positions slightly shifted to higher voltage leading to the disturbance in crystal structure because of lithiation and de-lithiation process. The overlapping of the CV curves from the 2nd to the 5th cycle highlights the material's good cycling stability and the reversible nature of the redox reactions [66, 75].



As the scan progresses, the diminishing differences between the curves from the 2nd cycle onward indicate the stabilization of the electrochemical reactions. This points to a reduction in the side reactions and higher coulombic efficiency in subsequent cycles, which is crucial for enhancing the performance of the anode in lithium-ion batteries.

Overall, the CV graph demonstrates the capacity of the SnS:ZnS@g-C₃N₄ composite to undergo reversible lithiation/de-lithiation with relatively low polarization, contributing to its potential as a high-performance anode material. The peaks' intensity and stability over multiple cycles reflect the material's ability to maintain consistent electrochemical activity, showing promise for long-term applications in rechargeable batteries.

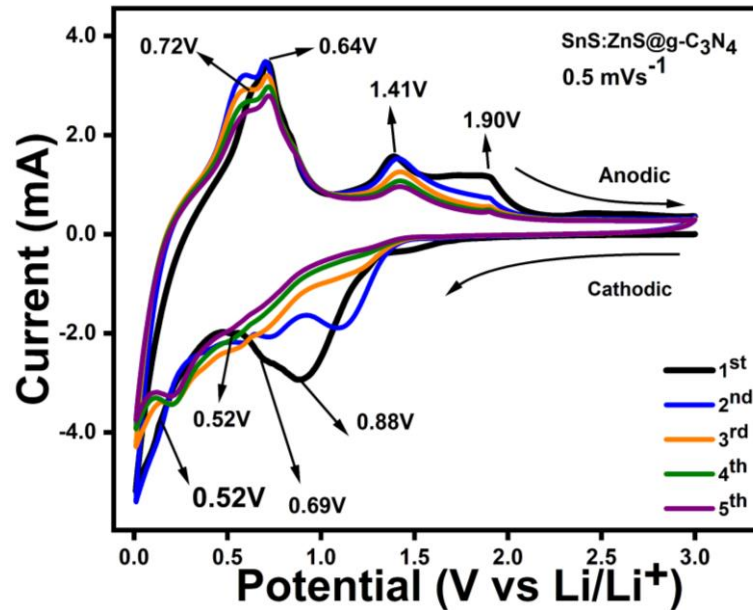


Figure 4.7: CV curves of SnS:ZnS on g-C₃N₄ at scan rate of 0.5 mVs⁻¹

4.2.2 Galvanostatic Charging and Discharging (GCD)

Figure 4.8 shows the galvanostatic charge-discharge profile of SnS:ZnS@g-C₃N₄ composite for 1st, 2nd, 3rd, 4th, and 5th cycle at current density 500 mA g⁻¹ in the voltage range of 0.01–3.0V with initial discharge capacities as 1624, 1015, 928, 849 and 844 mAhg⁻¹. For the first cycle the coulombic efficiency of SnS:ZnS@g-C₃N₄ electrode was found to measure approximately 60.86%. The capacity loss during the first cycle is attributed to the formation of solid electrolyte interphase layer (SEI) layer and some lithium-based byproducts generated at anode interface. During the first discharge, a broad plateau appearing at 0.88 V and a small peak at 0.69V 1.6V indicate the formation of the SEI layer along with the occurrence of irreversible reactions. After the 1st cycle, the coulombic efficiency of SnS:ZnS@g-C₃N₄ electrode rose to 98%, reflecting the high reversibility of the charge-discharge process. The peak situated at 0.52V and a shoulder at

0.13V assigned to conversion reactions of SnS and ZnS to their respective metal states (Sn and Zn), along with Li₂S formation. During the charge process another plateau appeared at around 1.7V indicating the de-alloying process. The galvanostatic charging and discharging (GCD) profiles agree well with CV curves of SnS:ZnS@g-C₃N₄. Pristine SnS:ZnS for five cycles, in strong agreement with one another. The discharge capacities of SnS:ZnS are calculated as 872, 590, 460 mAhg⁻¹. Obviously, SnS:ZnS@g-C₃N₄ electrode exhibits much enhanced specific capacity compared to SnS:ZnS, SnS and ZnS electrode which may be ascribed to different electrochemical behavior, as evident from CV and GCD profiles.

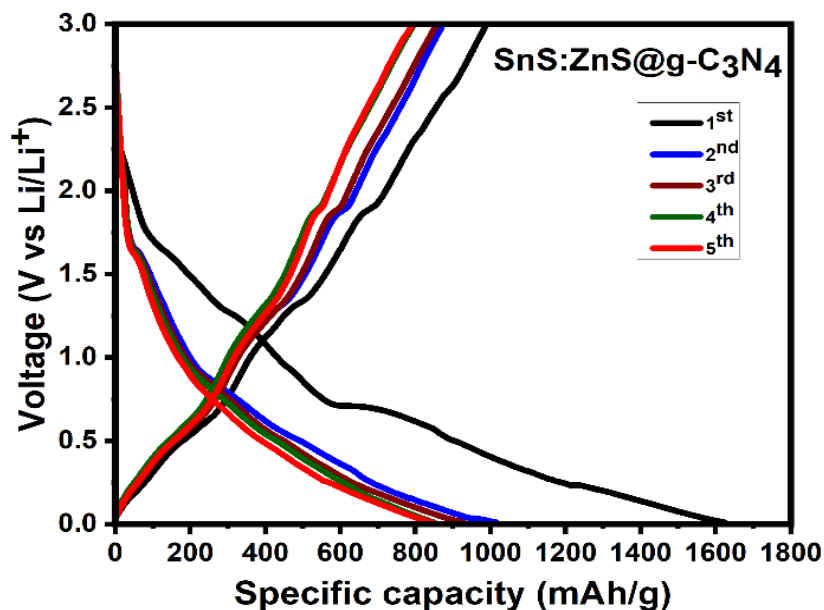


Figure 4.8: Galvanostatic charge-discharge curve of SnS:ZnS@g-C₃N₄

4.2.3 Rate Performance

To investigate the stability of synthesized electrode the rate performance test was conducted in the voltage range of 0.01–3.0 V at different scan rates represented in **Figure 4.9** SnS:ZnS@g-C₃N₄ reveals higher specific capacity with excellent stability. The specific capacities of SnS:ZnS@g-C₃N₄ at current densities (Ag⁻¹) or C-rates as 0.05, 0.1, 0.2, 0.3 0.5, 1.0 and 2.0 are 1623, 780, 697, 516, 417 and 329 mAhg⁻¹ respectively. When the current density returned to 0.3 Ag⁻¹ SnS:ZnS@g-C₃N₄ shows maximum reversible capacity 1045 mAhg⁻¹ at 800 cycles, after 800 cycles capacity gradually decreasing as cycles

number of increased. While at the same scan rate other electrodes such as ZnS/SnS, SnS and ZnS reveal lower reversible capacities like 366, 215 and 168 mA h g $^{-1}$ respectively. The reversible capacities of pristine material electrode decline sharply as compared to the ternary composite electrode as we move to higher current rates because during lithiation and de-lithiation volume expansion occurs up to 300% in alloy type anode material which leads to pulverization of active material and cause capacity fading. When we introduce the g-C $_3$ N $_4$ sheets which act as buffer layer and mitigate the volume expansion during the charging discharging of batteries, additional provides more channels for the li ions. The excellent high-rate performance of the ternary composites is attributed to their large surface area, abundant active sites, induced electric field, and 3D interconnected sheets like structure of g-C $_3$ N $_4$. This synergistic combination effectively boosts Li $^+$ ion diffusion pathways while simultaneously increasing the overall charge/discharge rate .

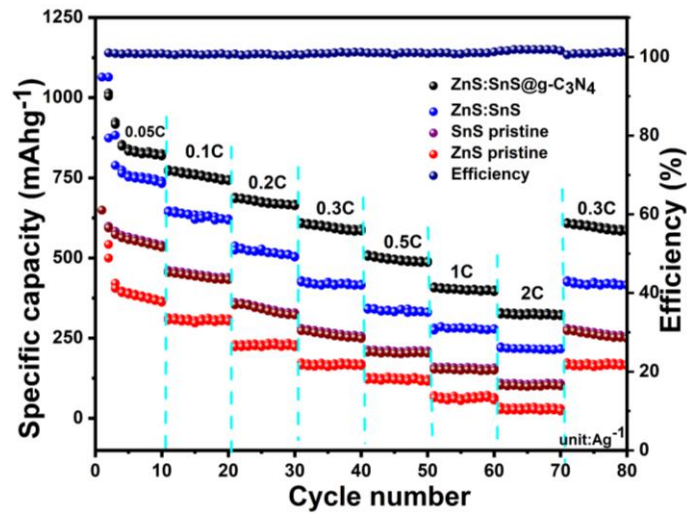


Figure 4.9: Rate capability comparison of ZnS, SnS, SnS:ZnS and SnS:ZnS@g-C $_3$ N $_4$ electrodes at various C-rates where 0.3C= 614 mA h g $^{-1}$

4.2.5 Cyclic stability

Figure 4.10 exhibits the cyclic stability profile at 0.3C (A g^{-1}) for SnS:ZnS@g-C $_3$ N $_4$, SnS:ZnS, SnS and ZnS electrodes. SnS:ZnS@g-C $_3$ N $_4$ tested for 1000 cycles in **Figure 4.11** indicating the prolong cyclic stability. While the rest of the electrodes reveal only 200 cycles at the same current density. The SnS:ZnS@g-C $_3$ N $_4$ shows higher reversible capacity with columbic efficiency 97.3%.

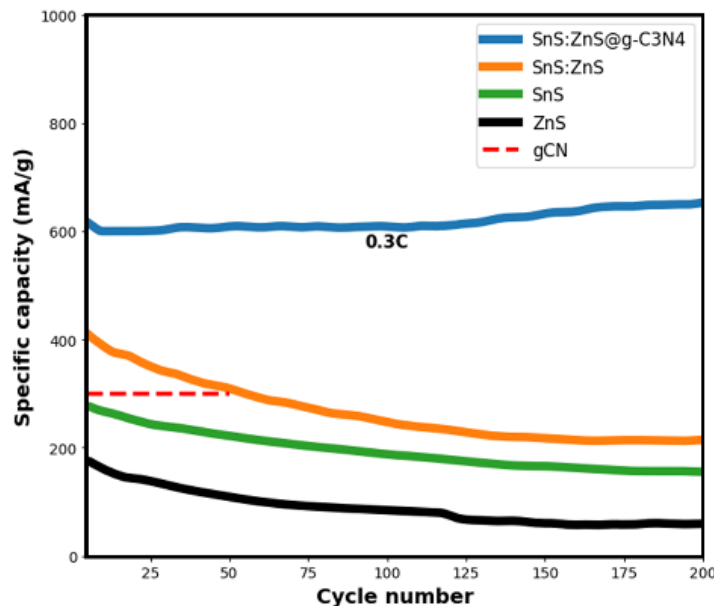


Figure 4.10: Cyclic performance comparison of ZnS, SnS, SnS:ZnS and SnS:ZnS@g-C₃N₄ electrodes at 0.3C

Therefore, it can be observed that SnS:ZnS nanoparticles anchored on g-C₃N₄ sheets deliver the optimal electrochemical performance which is mainly due to the enhanced density of active sites, larger surface area and built in electric field between SnS:ZnS interface which promotes the reaction kinetics. In figure 4.10 all anode materials are run for cyclic stability at 0.3 C-rate over the 200 cycles, pristine ZnS shows lower specific capacity due to volume expansion and material instability during lithiation and de lithiations. In case of SnS:ZnS specific capacity increase than single metal sulfide due to generation of built in electric field is induced when these two semiconductors came into account, after 100 cycles it starts decreasing the capacity due to pulverization of heterostructure. Finally, when we prepared a ternary composite SnS:ZnS@g-C₃N₄ which delivered initial 614 mAhg⁻¹. It is observed that after 100 cycles this electrode get activated and move towards higher capacity retentions to 1045 after 800 cycles shown in figure 4.11 which is due to the incorporations of g-C₃N₄ which act as a buffer layer mitigated the volume expansion occurs during battery operations and then gradually decrease with increasing the cycles [59].

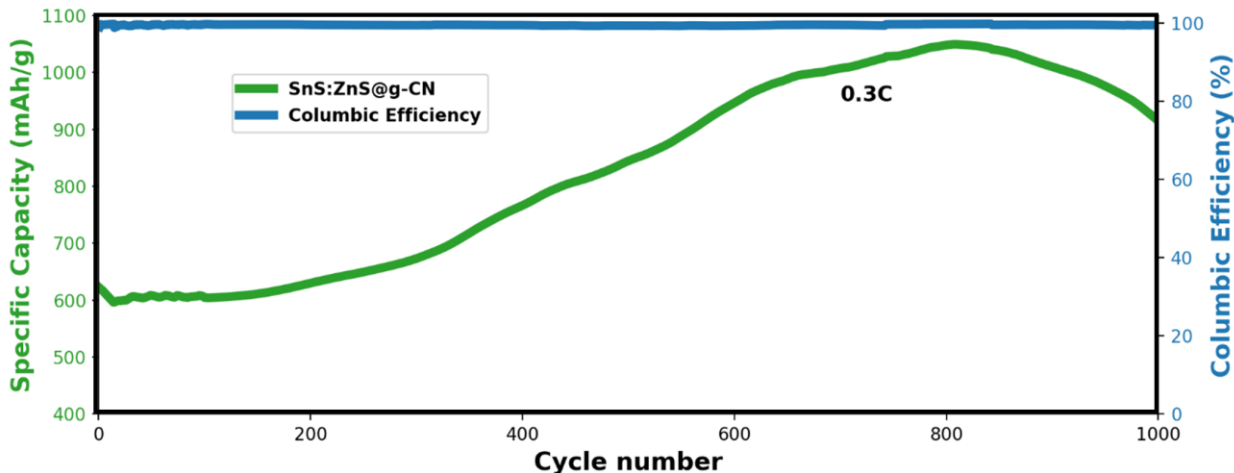


Figure 4.11: Prolong cyclic performance of SnS:ZnS@g-C₃N₄ at 0.3C for 1000 cycles.

4.2.5 EIS Testing

To probe the effect of g-C₃N₄ on the Li⁺ ion transport kinetics of SnS:ZnS@g-C₃N₄ electrode, EIS was conducted in the frequency range of 0.01 Hz to 100 KHz. **Figure 4.12** displays the Nyquist plots of SnS:ZnS@g-C₃N₄, SnS:ZnS, SnS and ZnS electrodes.

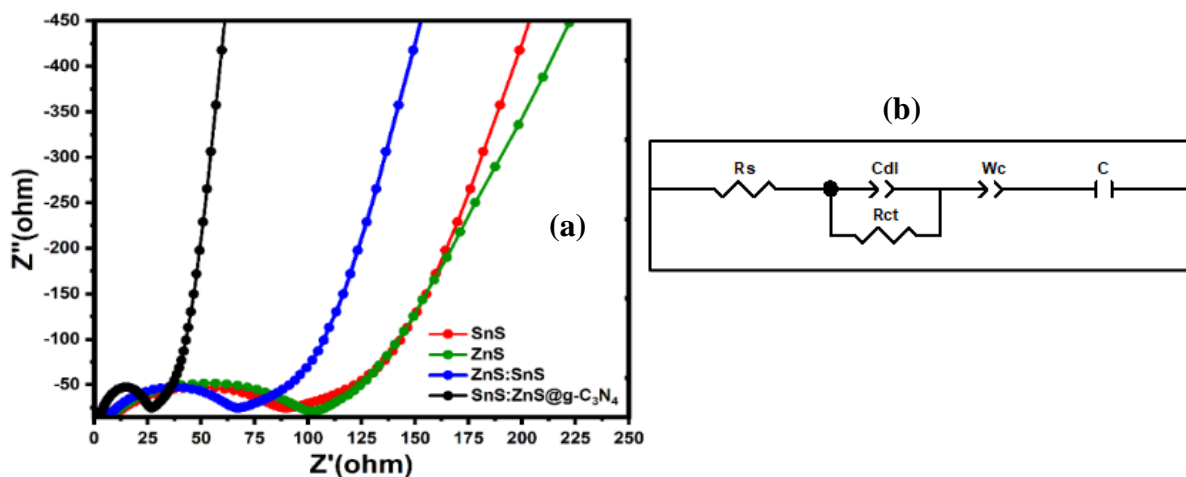


Figure 4.12: EIS Nyquist plot of pure SnS (red), ZnS (green), SnS:ZnS (blue) and SnS:ZnS@g-C₃N₄ (black) electrode calculated over the AC frequency range from 0.01 Hz to 100 kHz (a) and RC fitted equivalent circuit (b)

The suppressed semicircle observed in the high-frequency region is associated to the charge transfer resistance (R_{ct}) while the sloping straight line represents the Warburg coefficient (W_c) in the low-frequency region corresponding lithium-ion diffusion inside

the active material. Clearly, four electrode material electrodes exhibit depressed semicircles showing the non-ideal capacitive behavior. where R_s , R_{ct} , C_{dl} and W_c describe the solution

Table 4.1: EIS fitting parameters of ZnS, SnS, SnS:ZnS and SnS:ZnS@g-C₃N₄ electrodes.

Electrode	R_s (Ω)	R_{ct} (Ω)
ZnS	15.02	120.274
SnS	8.6	100.76
SnS:ZnS	5.3	60.05
SnS:ZnS@g-C ₃ N ₄	2.2	33.55

Resistance, charge transfer resistance for Li-ion signifies the associated component's capacitance, resistance, constant phase element and departure from the ideal Debye behavior, respectively.

The fitted equivalent circuit in the experimental data reveals one RC circuit in combination is connected in series with R_s and Warburg coefficient to describe the interfacial resistance between electrode and electrolyte while W_c gives the information of li-ion diffusion inside the material [93].

The fitting parameters, R_{ct} and R_s are presented in Table 4.1. The SnS:ZnS@g-C₃N₄ electrode possesses lower R_{ct} resistance 33.55 Ω as compared to other pristine electrodes. Evidently, the addition of g-C₃N₄ boosts the electrochemical performance and conductivity of the fabricated electrode material for LIBs.

4.3 Density Functional Theory (DFT)

4.3.1 *Siesta Calculations*

All calculations in this study were carried out using the numerical orbital method implemented in the SIESTA computational code (DFT). The Perdew-Burke-Ernzerhof (PBE) parameterization within the generalized gradient approximation (GGA) was applied as the exchange-correlation (XC) functional to account for electron-electron interactions in a system. Geometry optimization was considered complete when the forces on each atom were reduced to below 0.04 eV/\AA . The Monkhorst-Pack method, with a $6 \times 6 \times 6$ k-point grid, was employed to sample the Brillouin zone for calculating the density of states (DOS) and projected density of states (PDOS) as well as band structure. While a smaller DZP basis set was used for ZnS and SnS, potentially affecting the accuracy of the results, it allows for qualitative evaluation. A grid cut-off energy of 350 Ry was utilized for the self-consistent calculations of orthorhombic SnS and cubic ZnS [94].

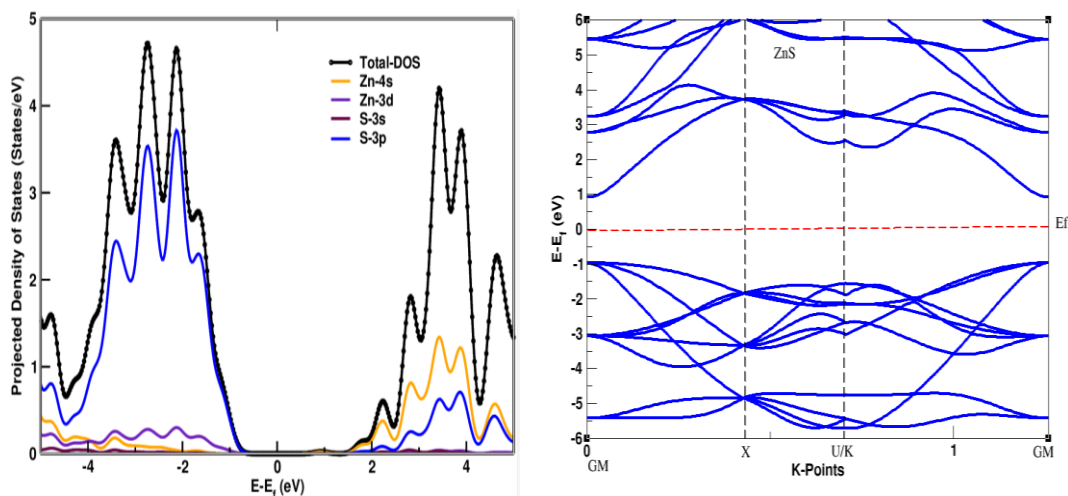


Figure 4.13: PDOS of pure ZnS (a) Bandgap of ZnS (b)

4.3.2 *Electrical Properties of ZnS by Siesta*

The electronic structure analysis of ZnS, with a band gap of $\sim 3.5 \text{ eV}$ as revealed by the band structure and PDOS shown in Figure 4.13, confirms its semiconducting nature [95].

The projected density of states (PDOS) shows significant contributions from Zn 3d and S 3p orbitals in the valence band and in conduction band larger contributions of Zn 4s

and S-3p while no states are present at the Fermi level, indicating low electronic conductivity. This limitation can hinder the fast electron transport required for high-rate performance in battery applications [68].

Despite this, ZnS is still valuable as an anode material due to its strong ionic conductivity and structural stability, which arise from the hybridization between Zn and S orbitals. The large band gap also suggests good cycling stability, reducing unwanted side reactions.

To optimize ZnS for battery use, it is often combined with conductive materials like SnS or any carbon material like g-C₃N₄, improving its overall conductivity while maintaining its electrochemical stability, making it suitable for long-term energy storage applications.

4.3.3 *Electrical Properties of SnS by Siesta*

The electronic properties analysis for SnS, as shown by the PDOS and band structure, indicates that SnS is also a semiconductor in Figure . The **PDOS** reveals key contributions from both Sn and S orbitals, with the Sn 5p (green) and S 3p (blue) orbitals dominating the valence band just below the Fermi level.

The Sn 5s (red) and Sn 4d (purple) states are less prominent but still contribute to deeper energy levels. Importantly, there are no states at the Fermi level (E_{F}), confirming the semiconducting nature of SnS, which could limit its electronic conductivity in battery applications.

The **band structure** plot further confirms this, showing a clear separation between the valence and conduction bands, with a band gap in the range of ~1–2 eV [96]. This is smaller than that of ZnS, suggesting better intrinsic electronic conductivity compared to ZnS.

However, for efficient use in battery anodes, SnS may still require the incorporation of conductive additives to enhance its performance, especially in high-rate applications. Its relatively narrow band gap and good ionic conductivity make it a promising candidate for energy storage, offering a balance between cycling stability and electronic performance.

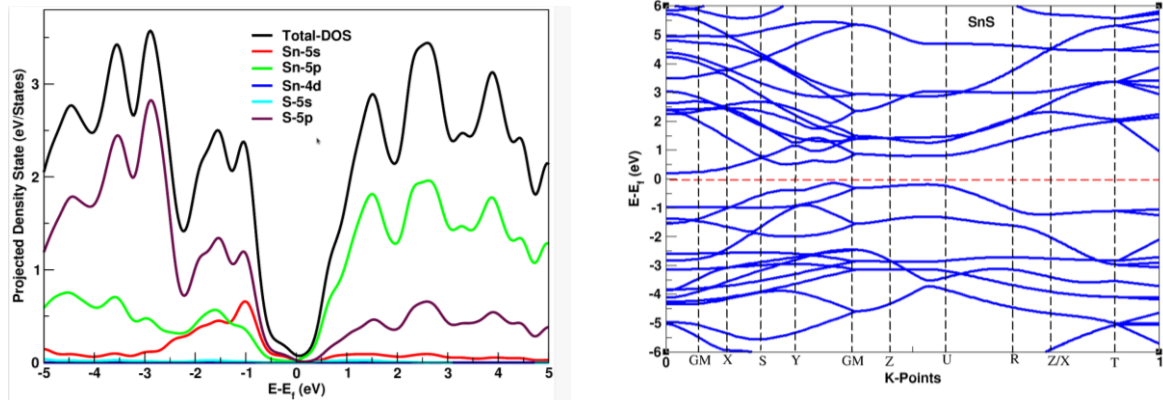


Figure 4.14: PDOS of pure SnS (a) Bandgap of SnS (b)

4.3.4 Heterostructure of SnS:ZnS

In the SnS:ZnS heterostructure, the difference in their electronic properties, such as band gap and work function, creates a built-in electric field at the interface. This field arises due to band bending, which occurs as the Fermi levels of SnS and ZnS equilibrate.

The band offset between SnS (narrower band gap ~ 1.1 eV) and ZnS (wider band gap ~ 3.6) causes the conduction and valence bands to align in a staggered (Type-II) configuration [63].

This alignment promotes the spatial separation of electrons and holes, which enhances charge carrier mobility and reduces recombination losses. As a result, electron transport across the heterojunction becomes more efficient.

For battery performance, this built-in electric field facilitates faster electron transfer during charge and discharge cycles. It can also assist in improving ionic diffusion by preventing charge buildup, which commonly limits the electrode's electrochemical kinetics [76].

This results in enhanced rate capability, higher energy density, and improved cycling stability. Additionally, the presence of the heterostructure improves the structural integrity of the anode, preventing degradation during repeated lithiation/de-lithiation or processes, further boosting the long-term stability of the alloy type battery.

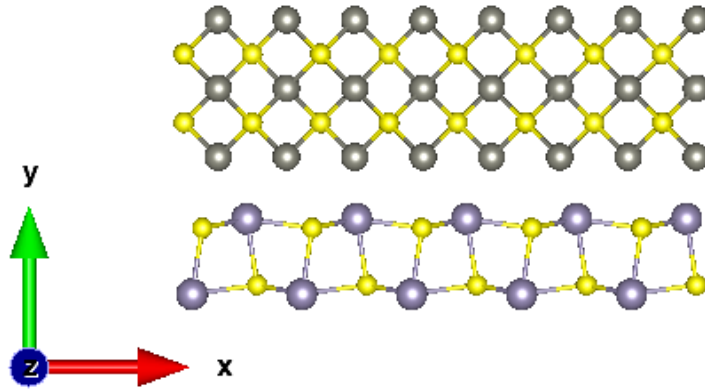


Figure 4.15: Heterostructure of SnS:ZnS

CHAPTER 5: CONCLUSIONS AND FUTURE RECOMMENDATION

5.1 Conclusion

In conclusion, we have synthesized the $\text{SnS:ZnS@g-C}_3\text{N}_4$ composite via a facile solvothermal process. Among the different electrodes, the $\text{SnS:ZnS@g-C}_3\text{N}_4$ demonstrates prolonged cyclability and capacity retention as an anode for LIBs. With an initial discharge capacity of 1623 mAhg^{-1} and reached remarkable cycling stability, retaining 1045 mAhg^{-1} over 800 cycles at 0.3C, it outperforms than pristine SnS:ZnS, ZnS, and SnS anodes. The SnS:ZnS heterostructure's synergy effectively mitigates volume expansion produced during lithiation and de-lithiations, while electrochemical impedance spectroscopy (EIS) reveals significantly reduced interfacial resistance for ternary composite as $\text{SnS:ZnS@g-C}_3\text{N}_4$ which is 33.1Ω , enhancing Li-ion diffusion and reaction kinetics. This composite offers a strategic pathway to advanced, high-capacity, and stable anode materials for next-generation LIBs, addressing key challenges associated with alloy type anode in battery technology.

5.2 Future Recommendations

- For the future Prospective, different cost-effective synthesis methods can be utilized rather than Solvothermal.
- $\text{SnS:ZnS@g-C}_3\text{N}_4$ material can be tested for solid State batteries, can be tested for Na-ion batteries Operando study by using XRD synchrotron,
- Electrochemical quartz crystal microbalance (EQCM) can be utilized for the real time analysis during battery operations.

REFERENCES

- [1] B. Scrosati and J. Garche, "Lithium batteries: Status, prospects and future," *Journal of power sources*, vol. 195, no. 9, pp. 2419-2430, 2010.
- [2] N. R. Council, D. o. Engineering, P. Sciences, B. o. A. Science, and C. o. S. P. E. Systems, "Meeting the energy needs of future warriors," 2004.
- [3] J. A. Laddusaw, A. G. Pollman, O. A. Yakimenko, and A. J. Gannon, "Combining a Fuel Cell and Ultracapacitor Bank to Power a Vertical Take-Off and Landing Unmanned Aerial System," in *ASME Power Conference*, 2020, vol. 83747, p. V001T10A007: American Society of Mechanical Engineers.
- [4] A. Yoshino, "The birth of the lithium-ion battery," *Angewandte Chemie International Edition*, vol. 51, no. 24, pp. 5798-5800, 2012.
- [5] M. D. Slater, D. Kim, E. Lee, and C. S. Johnson, "Sodium-ion batteries," *Advanced Functional Materials*, vol. 23, no. 8, pp. 947-958, 2013.
- [6] T. Pamulapati, M. Cavus, I. Odigwe, A. Allahham, S. Walker, and D. Giaouris, "A review of microgrid energy management strategies from the energy trilemma perspective," *Energies*, vol. 16, no. 1, p. 289, 2022.
- [7] J. Zhao and A. F. Burke, "Electrochemical capacitors: Materials, technologies and performance," *Energy Storage Materials*, vol. 36, pp. 31-55, 2021.
- [8] Y. Huang *et al.*, "Interfaces Engineering Toward Stable Lithium-Sulfur Batteries," *Energy & Environmental Science*, 2024.
- [9] K. Pan *et al.*, "Integrated data mining for prediction of specific capacitance of porous carbon materials for flexible energy storage devices," *Journal of Energy Storage*, vol. 73, p. 109072, 2023.
- [10] E. Fan *et al.*, "Sustainable recycling technology for Li-ion batteries and beyond: challenges and future prospects," *Chemical reviews*, vol. 120, no. 14, pp. 7020-7063, 2020.
- [11] U.-H. Kim *et al.*, "Cation ordered Ni-rich layered cathode for ultra-long battery life," *Energy & Environmental Science*, vol. 14, no. 3, pp. 1573-1583, 2021.
- [12] N.-S. Popa, C. Popa, V. Mocanu, and L.-M. POPA, "State of the Art in Battery Technology: Innovations and Advancements," *Journal of Marine Technology and Environment*, pp. 81-85, 2023.

- [13] G. G. Eshetu *et al.*, "Electrolytes and interphases in sodium-based rechargeable batteries: recent advances and perspectives," *Advanced Energy Materials*, vol. 10, no. 20, p. 2000093, 2020.
- [14] M. Hannan, M. M. Hoque, A. Mohamed, and A. Ayob, "Review of energy storage systems for electric vehicle applications: Issues and challenges," *Renewable and Sustainable Energy Reviews*, vol. 69, pp. 771-789, 2017.
- [15] N. Yabuuchi, K. Kubota, M. Dahbi, and S. Komaba, "Research development on sodium-ion batteries," *Chemical reviews*, vol. 114, no. 23, pp. 11636-11682, 2014.
- [16] J. Khan *et al.*, "2-formyl-3, 6-bis (hydroxymethyl) phenyl benzoate in Electrochemical Dry Cell," *Open Chemistry*, vol. 16, no. 1, pp. 912-917, 2018.
- [17] Y. Wang *et al.*, "Lithium and lithium ion batteries for applications in microelectronic devices: A review," *Journal of Power Sources*, vol. 286, pp. 330-345, 2015.
- [18] M. M. Thackeray, C. Wolverton, and E. D. Isaacs, "Electrical energy storage for transportation—approaching the limits of, and going beyond, lithium-ion batteries," *Energy & Environmental Science*, vol. 5, no. 7, pp. 7854-7863, 2012.
- [19] Q. Dai, J. C. Kelly, L. Gaines, and M. Wang, "Life cycle analysis of lithium-ion batteries for automotive applications," *Batteries*, vol. 5, no. 2, p. 48, 2019.
- [20] C. Glaize and S. Geniès, "Accumulateurs au lithium, haute température et à circulation d'électrolyte," ed, 2013.
- [21] M. S. Whittingham, "Electrical energy storage and intercalation chemistry," *Science*, vol. 192, no. 4244, pp. 1126-1127, 1976.
- [22] J.-M. Tarascon and M. Armand, "Issues and challenges facing rechargeable lithium batteries," *nature*, vol. 414, no. 6861, pp. 359-367, 2001.
- [23] <https://www.securities.io/investing-nobel-prize-lithium-ion-batteries-to-power-the-world/>.
- [24] T. N. K. Tozawa and T. Tozawa, "Lithium ion rechargeable battery. Prog. Batter," *Solar. Cells*, vol. 9, p. 209, 1990.
- [25] K. Ozawa, "Lithium-ion rechargeable batteries with LiCoO₂ and carbon electrodes: the LiCoO₂/C system," *Solid State Ionics*, vol. 69, no. 3-4, pp. 212-221, 1994.
- [26] Z. Wang *et al.*, "Disordered materials for high-performance lithium-ion batteries: A review," *Nano Energy*, p. 109250, 2024.
- [27] R. Maghsoudi, A. Ghezi, S. Jamalpour, Y. Tamsilian, M. Tohidian, and Y. Shahebrahimi, "Advantages, Limitations, and Industrial Applications of Lithium-

- Ion Batteries," *Nanostructured Materials for Energy Storage*, vol. 2, pp. 793-820, 2024.
- [28] W. Li *et al.*, "Recent progress of self-supported anode materials for Li-ion batteries," *Journal of Energy Storage*, vol. 99, p. 113188, 2024.
- [29] K. Sashmitha and M. U. Rani, "A comprehensive review of polymer electrolyte for lithium-ion battery," *Polymer Bulletin*, vol. 80, no. 1, pp. 89-135, 2023.
- [30] D. Ding, Y. Maeyoshi, M. Kubota, J. Wakasugi, K. Kanamura, and H. Abe, "Non-flammable super-concentrated polymer electrolyte with "solvated ionic liquid" for lithium-ion batteries," *Journal of Power Sources*, vol. 506, p. 230099, 2021.
- [31] R. Wang *et al.*, "Effect of different binders on the electrochemical performance of metal oxide anode for lithium-ion batteries," *Nanoscale research letters*, vol. 12, pp. 1-11, 2017.
- [32] H. Liu *et al.*, "Sn-based anode materials for lithium-ion batteries: From mechanism to modification," *Journal of Energy Storage*, vol. 80, p. 109862, 2024.
- [33] B. E. Murdock, K. E. Toghil, and N. Tapia-Ruiz, "A perspective on the sustainability of cathode materials used in lithium-ion batteries," *Advanced Energy Materials*, vol. 11, no. 39, p. 2102028, 2021.
- [34] Y. K. Liu, C. Z. Zhao, J. Du, X. Q. Zhang, A. B. Chen, and Q. Zhang, "Research Progresses of Liquid Electrolytes in Lithium-Ion Batteries," *Small*, vol. 19, no. 8, p. 2205315, 2023.
- [35] Y. Liao and W. Li, "Separators for lithium ion batteries," in *Advanced Materials for Battery Separators*: Elsevier, 2024, pp. 73-140.
- [36] S. Shahid and M. Agelin-Chaab, "A review of thermal runaway prevention and mitigation strategies for lithium-ion batteries," *Energy Conversion and Management: X*, vol. 16, p. 100310, 2022.
- [37] A. Masias, J. Marcicki, and W. A. Paxton, "Opportunities and challenges of lithium ion batteries in automotive applications," *ACS energy letters*, vol. 6, no. 2, pp. 621-630, 2021.
- [38] S. H. Park, J. Park, M.-H. Ryou, and Y. M. Lee, "Sensitivity of power of lithium-ion batteries to temperature: A case study using cylindrical-and pouch-type cells," *Journal of Power Sources*, vol. 465, p. 228238, 2020.
- [39] M. Alipour, C. Ziebert, F. V. Conte, and R. Kizilel, "A review on temperature-dependent electrochemical properties, aging, and performance of lithium-ion cells," *Batteries*, vol. 6, no. 3, p. 35, 2020.

- [40] J. Huisman, T. Ciuta, F. Mathieux, S. Bobba, K. Georgitzikis, and D. Pennington, "RMIS—Raw materials in the battery value chain," *Publications Office of the European Union, Luxembourg*, 2020.
- [41] N. Omar *et al.*, "Aging and degradation of lithium-ion batteries," in *Rechargeable lithium batteries*: Elsevier, 2015, pp. 263-279.
- [42] J. Guo, Y. Li, K. Pedersen, and D.-I. Stroe, "Lithium-ion battery operation, degradation, and aging mechanism in electric vehicles: An overview," *Energies*, vol. 14, no. 17, p. 5220, 2021.
- [43] A. Glibo, N. Eshraghi, Y. Surace, A. Mautner, H. Flandorfer, and D. M. Cupid, "Comparative study of electrochemical properties of SnS and SnS₂ as anode materials in lithium-ion batteries," *Electrochimica Acta*, vol. 441, p. 141725, 2023.
- [44] D. D. Pathak, D. P. Dutta, B. R. Ravuri, A. Ballal, A. C. Joshi, and A. K. Tyagi, "An insight into the effect of g-C₃N₄ support on the enhanced performance of ZnS nanoparticles as anode material for lithium-ion and sodium-ion batteries," *Electrochimica Acta*, vol. 370, p. 137715, 2021.
- [45] S. Palchoudhury, K. Ramasamy, J. Han, P. Chen, and A. Gupta, "Transition metal chalcogenides for next-generation energy storage," *Nanoscale Advances*, vol. 5, no. 10, pp. 2724-2742, 2023.
- [46] P. Nzereogu, A. Omah, F. Ezema, E. Iwuoha, and A. Nwanya, "Anode materials for lithium-ion batteries: A review," *Applied Surface Science Advances*, vol. 9, p. 100233, 2022.
- [47] T. M. Gür, "Materials and technologies for energy storage: Status, challenges, and opportunities," *MRS bulletin*, vol. 46, no. 12, pp. 1153-1163, 2021.
- [48] K. Roy, A. Banerjee, and S. Ogale, "Search for new anode materials for high performance Li-ion batteries," *ACS Applied Materials & Interfaces*, vol. 14, no. 18, pp. 20326-20348, 2022.
- [49] T. S. Munonde and M. C. Raphulu, "Review on titanium dioxide nanostructured electrode materials for high-performance lithium batteries," *Journal of Energy Storage*, vol. 78, p. 110064, 2024.
- [50] P. N. Suryadi, J. Karunawan, O. Floweri, and F. Iskandar, "Toward high-rate capability of intercalation cathodes Li-ion batteries, potency for fast-charging application: A materials perspective," *Journal of Energy Storage*, vol. 68, p. 107634, 2023.
- [51] S. Kannan, A. Thirumurugan, R. K. Pai, and A. Ramadoss, "Benchmarking Electrode Materials for High-Energy Lithium-Ion Batteries," *Nanostructured Materials for Energy Storage*, vol. 1, pp. 33-73, 2024.

- [52] Y. Lu, L. Yu, and X. W. D. Lou, "Nanostructured conversion-type anode materials for advanced lithium-ion batteries," *Chem*, vol. 4, no. 5, pp. 972-996, 2018.
- [53] V. Etacheri, R. Marom, R. Elazari, G. Salitra, and D. Aurbach, "Challenges in the development of advanced Li-ion batteries: a review," *Energy & Environmental Science*, vol. 4, no. 9, pp. 3243-3262, 2011.
- [54] X. Hu *et al.*, "Interface and structure engineering of tin-based chalcogenide anodes for durable and fast-charging sodium ion batteries," *Advanced Energy Materials*, vol. 12, no. 47, p. 2202318, 2022.
- [55] M. A. Rahman, G. Song, A. I. Bhatt, Y. C. Wong, and C. Wen, "Nanostructured silicon anodes for high-performance lithium-ion batteries," *Advanced Functional Materials*, vol. 26, no. 5, pp. 647-678, 2016.
- [56] W. Zhang *et al.*, "Facile synthesis of ZnS nanoparticles decorated on defective CNTs with excellent performances for lithium-ion batteries anode material," *Journal of Alloys and Compounds*, vol. 816, p. 152633, 2020.
- [57] A. Mayyas, A. Chadly, S. T. Amer, and E. Azar, "Economics of the Li-ion batteries and reversible fuel cells as energy storage systems when coupled with dynamic electricity pricing schemes," *Energy*, vol. 239, p. 121941, 2022.
- [58] H. Wang, Y. Deng, W. Zhang, and S. Yao, "Cerium-doped SnS micron flowers with long life and high capacity for hybrid supercapacitors," *Journal of Alloys and Compounds*, vol. 976, p. 173402, 2024.
- [59] D. Cheng, M. Lin, J. Liu, L. Yang, Y. Chen, and M. Zhu, "N-doped carbon coated SnS/rGO composite with superior cyclic stability as anode for lithium-ion batteries," *Industrial & Engineering Chemistry Research*, vol. 61, no. 12, pp. 4339-4347, 2022.
- [60] H.-C. Tao, X.-L. Yang, L.-L. Zhang, and S.-B. Ni, "One-step in situ synthesis of SnS/graphene nanocomposite with enhanced electrochemical performance for lithium ion batteries," *Journal of Electroanalytical Chemistry*, vol. 728, pp. 134-139, 2014.
- [61] A. A. Qayyum, Z. S. Khan, S. Ashraf, and N. Ahmed, "Amorphous codoped SnS/CNTs nanocomposite with improved capacity retention as an advanced sodium-ion battery anode," *Journal of Materials Science: Materials in Electronics*, vol. 31, pp. 14521-14530, 2020.
- [62] H. Tang *et al.*, "Construction of Ti₃C₂ MXene@ C@ SnS with layered rock stratum structure for high-performance lithium storage," *Journal of Power Sources*, vol. 462, p. 228152, 2020.

- [63] Z. Dang, W. Meng, J. Han, D. Li, and L. Jiang, "In-situ vulcanization synthesis of honeycomb-like SnS/C nanocomposites as anode materials for lithium-ion batteries," *Journal of Alloys and Compounds*, vol. 891, p. 162051, 2022.
- [64] D. Cheng, L. Yang, R. Hu, J. Cui, J. Liu, and M. Zhu, "Construction of SnS-Mo-graphene nanosheets composite for highly reversible and stable lithium/sodium storage," *Journal of Materials Science & Technology*, vol. 121, pp. 190-198, 2022.
- [65] C. Zhang *et al.*, "Boosting sodium-ion storage via the thermodynamic-and dynamic-induced bidirectional interfacial electric field in the ZnS/Sn₂S₃ heterostructure anode," *Energy & Fuels*, vol. 36, no. 23, pp. 14423-14432, 2022.
- [66] P. Xu *et al.*, "Honeycomb substrate carbon and nitrogen-doped coated carbon synergistically boost SnS/ZnS for efficient lithium storage," *Materials Letters*, vol. 357, p. 135710, 2024.
- [67] T. Xiao *et al.*, "In-situ growth of flake SnS in three-dimensional hierarchical porous carbon boosting lithium storage performance," *Journal of Energy Storage*, vol. 78, p. 109897, 2024.
- [68] H. Peng *et al.*, "Reducing polarization of lithium-sulfur batteries via ZnS/reduced graphene oxide accelerated lithium polysulfide conversion," *Materials Today Energy*, vol. 18, p. 100519, 2020.
- [69] M. Cao *et al.*, "Rational design of ZnS/CoS heterostructures in three dimensional N-doped CNTs for superior lithium storage," *Journal of Alloys and Compounds*, vol. 859, p. 157867, 2021.
- [70] X. Luo, J. Shao, P. He, K. Li, and W. Zhao, "Construction of hierarchical ZnS/MoS₂ bimetallic sulfides heterostructures for high-performance sodium ion batteries," *Applied Surface Science*, vol. 607, p. 154821, 2023.
- [71] H. Zhang *et al.*, "Heterostructured ZnS/Co embedded in pinecone-like N/S-doped carbon for efficient sodium/lithium storage," *Chemical Engineering Journal*, vol. 489, p. 151318, 2024.
- [72] J. Hu, J. Li, X. Gao, J. Shi, and K. Yu, "Effect of BaSO₄ additive on cycling performance of ZnS/C-SnO₂ for advanced sodium-ion batteries," *Materials Chemistry and Physics*, vol. 312, p. 128584, 2024.
- [73] M. L. Chen *et al.*, "A Facile Cation-Exchange Strategy for ZnS-SnS-Sb₂S₃@ C Submicron Box as Advanced Anode for Li-Ion Batteries," *ChemNanoMat*, vol. 9, no. 3, p. e202200540, 2023.
- [74] L. Zhang *et al.*, "Rationally designed heterostructure ZnS/SnS@ N-doped carbon microspheres as high-performance anode for lithium-ion batteries," *Journal of Alloys and Compounds*, vol. 910, p. 164908, 2022.

- [75] D. Bian, X. Cheng, H. Li, S. Qiao, and X. Wang, "Heterointerface engineering of hierarchical SnS/ZnS with Rich Phase Boundaries rich phase boundaries for superior sodium storage performance," *Journal of Alloys and Compounds*, vol. 919, p. 165577, 2022.
- [76] W. Yao *et al.*, "ZnS-SnS@ NC heterostructure as robust lithiophilicity and sulfiphilicity mediator toward high-rate and long-life lithium–sulfur batteries," *ACS nano*, vol. 15, no. 4, pp. 7114-7130, 2021.
- [77] Q. Liang *et al.*, "Heterostructured SnS-ZnS@ C nanoparticles embedded in expanded graphite as advanced anode materials for lithium ion batteries," *Chemical Physics Letters*, vol. 775, p. 138662, 2021.
- [78] A. Sadaqat, G. Ali, Z. Ali, F. J. Iftikhar, and M. u. Hasan, "Synergetic effect of binary ZnS: SnS composites with reduced graphene oxide and carbon nanotubes as anodes for sodium-ion batteries," *ACS Applied Energy Materials*, vol. 4, no. 12, pp. 13868-13877, 2021.
- [79] J. Ai *et al.*, "Pomegranate-inspired SnS/ZnS@ C heterostructural nanocubes towards high-performance sodium ion battery," *Applied Surface Science*, vol. 496, p. 143631, 2019.
- [80] Y. Zhang *et al.*, "Heterostructured SnS-ZnS@ C hollow nanoboxes embedded in graphene for high performance lithium and sodium ion batteries," *Chemical Engineering Journal*, vol. 356, pp. 1042-1051, 2019.
- [81] P. Sakthi, J. Uma, C. Siva, and B. Balraj, "Efficient charge transport and enhanced photocatalysis of ultrasonically decorated SnS QDs on g-C3N4 nanosheets," *Journal of Materials Science: Materials in Electronics*, vol. 34, no. 3, p. 204, 2023.
- [82] L. Tan, J. Xu, X. Zhang, Z. Hang, Y. Jia, and S. Wang, "Synthesis of g-C3N4/CeO2 nanocomposites with improved catalytic activity on the thermal decomposition of ammonium perchlorate," *Applied Surface Science*, vol. 356, pp. 447-453, 2015.
- [83] D. Feng *et al.*, "Enhanced photocatalytic activities of g-C3N4 with large specific surface area via a facile one-step synthesis process," *Carbon*, vol. 125, pp. 454-463, 2017.
- [84] A. Sewnet *et al.*, "Single-step synthesis of graphitic carbon nitride nanomaterials by directly calcining the mixture of urea and thiourea: application for rhodamine B (RhB) dye degradation," *Nanomaterials*, vol. 13, no. 4, p. 762, 2023.
- [85] Y. Jin *et al.*, "Study on colloidal synthesis of ZnS nanospheres embedded in reduced graphene oxide materials for sodium-ion batteries and energy storage mechanism," *Journal of Alloys and Compounds*, vol. 943, p. 169076, 2023.
- [86] X. Yuan, S. Qiu, and X. Zhao, "Covalent fixing of MoS2 nanosheets with SnS nanoparticles anchored on g-C3N4/graphene boosting fast charge/ion transport for

- sodium-ion hybrid capacitors," *ACS Applied Materials & Interfaces*, vol. 13, no. 29, pp. 34238-34247, 2021.
- [87] Y. Tang, X. Wang, J. Chen, X. Wang, D. Wang, and Z. Mao, "Templated transformation of g-C₃N₄ nanosheets into nitrogen-doped hollow carbon sphere with tunable nitrogen-doping properties for application in Li-ions batteries," *Carbon*, vol. 168, pp. 458-467, 2020.
- [88] S. A. Thomas, M. R. Pallavolu, M. E. Khan, and J. Cherusseri, "Graphitic carbon nitride (g-C₃N₄): Futuristic material for rechargeable batteries," *Journal of Energy Storage*, vol. 68, p. 107673, 2023.
- [89] B. A. Shah, S. T. U. Din, A. Sardar, S. Daud, and B. Yuan, "Polydopamine@ SnS/g-C₃N₄ heterojunction photocatalyst: Insight into visible-light-induced reactive oxygen species (ROS)-mediated antibacterial and antimold activities," *Journal of Environmental Chemical Engineering*, vol. 10, no. 6, p. 108655, 2022.
- [90] H. A. Omr *et al.*, "Design of sculptured SnS/g-C₃N₄ photocatalytic nanostructure for highly efficient and selective CO₂ conversion to methane," *Applied Catalysis B: Environmental*, vol. 324, p. 122231, 2023.
- [91] B. Liu *et al.*, "Boosting O₂ reduction and H₂O dehydrogenation kinetics: surface N-hydroxymethylation of g-C₃N₄ photocatalysts for the efficient production of H₂O₂," *Advanced Functional Materials*, vol. 32, no. 15, p. 2111125, 2022.
- [92] C. Wang *et al.*, "Construction of uniform SnS₂/ZnS heterostructure nanosheets embedded in graphene for advanced lithium-ion batteries," *Journal of Alloys and Compounds*, vol. 820, p. 153147, 2020.
- [93] W. Choi, H.-C. Shin, J. M. Kim, J.-Y. Choi, and W.-S. Yoon, "Modeling and applications of electrochemical impedance spectroscopy (EIS) for lithium-ion batteries," *Journal of Electrochemical Science and Technology*, vol. 11, no. 1, pp. 1-13, 2020.
- [94] D. A. Kolosov and O. E. Glukhova, "Ab Initio Study of Porous Graphene–CNT Silicon Composite for Li-Ion and Na-Ion Batteries," *C*, vol. 7, no. 3, p. 57, 2021.
- [95] S. Sharma, A. Shrivastav, A. Oudhia, and M. L. Verma, "A First principle study of structural and electronic properties of ZnO and ZnS Buckyball structures," in *IOP Conference Series: Materials Science and Engineering*, 2020, vol. 798, no. 1, p. 012032: IOP Publishing.
- [96] N. S. Kozhevnikova *et al.*, "A facile low-temperature deposition of Sn-rich tin (II) monosulfide colloid particles," *Наносистемы: физика, химия, математика*, vol. 11, no. 5, pp. 529-536, 2020.